Calculation of Subsynchronous Shaft Oscillations from Terminal Voltage in Multimass Turbine – Generators

presented to the
Faculty of Graduate Studies
The University of Manitoba
in partial fulfilment of
the requirements for the degree
Master of Science
in Electrical Engineering

by
Peter W. Lehn
Department of Electrical and Computer Engineering
University of Manitoba

Winnipeg, Manitoba, 1992

ISBN 0-315-81779-8

CALCULATION OF SUBSYNCHRONOUS SHAFT OSCILLATIONS FROM TERMINAL VOLTAGE IN MULTIMASS TURBINE-GENERATORS

BY

PETER W. LEHN

A Thesis submitted to the Faculty of Graduate Studies of the University of Manitoba in partial fulfillment of the requirements for the degree of

MASTER OF SCIENCE

Abstract

Subsynchronous resonance is a phenomenon which occurs in a host of power system configurations. Often subsynchronous oscillations initiate torsional interactions between the masses of a multimass turbine–generator. In many systems the mechanical shaft oscillations must be measured for control purposes.

In this thesis, a new technique is developed to determine the amplitude of these oscillations. The technique is based on the Fourier Transform of the machine's teminal voltage. A useful relation between the voltage frequency spectrum and the mechanical oscillation amplitudes is derived and tested. Verification of the theory is carried out using EMTDC simulation for a variety of network configurations.

Acknowledgements

I wish to thank Dr. A. Gole for his guidance, encouragement and patience throughout the course of this thesis.

I am also indebted to Mr. D. Menzies of ABB for his helpful suggestions and for the use of his extensive reference materials.

I gratefully acknowledge the financial support of NSERC, in the form of a postgraduate scholarship.

Table of Contents

List of Figures

List of Tables

Chapter 1

Introduction

1 .1 Motivation

Subsynchronous resonance (SSR) is a phenomenon which occurs in a variety of power system schemes. Predominantly, SSR exists in systems which either contain long series compensated lines or employ HVDC links. The pssibility exists, however, for almost any system to display SSR effects of some type, if the system is not appropriately designed. An official definition for SSR was proposed by the IEEE SSR working group in 1980 [1]:

"SSR is an electric power system condition where the electric network exchanges energy with a turbine generator at one or more of the natural frequencies of the combined system below the synchronous frequency of the system."

This type of resonance may appear in a system for a number of reasons, including self–excitation, torsional interactions and DC converter control interactions.

1 .2 Background

Until the introduction of HVDC transmission systems, SSR was primarily due to an abundance of series compensation in long EHV AC

transmission lines. Already in the 1930's, series capacitors were described to be one of the most efficient ways of increasing the transmission capacity for long lines. Unfortunately, experimentation with series capacitors proved much less ideal than expected, and many papers were written on the stability problems associated with the use of these capacitors. Generally, the stability problems were attributed to self–excitation [2] and the negative damping [3] introduced by nearby generating units. A few of the instabilities were attributed to other factors, such as ferroresonance [4].

In 1970, however, a great deal of attention was suddenly focussed on the effects of torsional interactions in the generator/turbine shaft. This was most likely due to the actual shaft failure which occurred at the Mohave Generating Station in southern California [5]. Since that time many papers have been written on the prediction and control of subsynchronous torsional interactions.

In 1977 torsional interactions between a turbine–generator and an HVDC link were observed during tests at Square Butte in North Dakota [6]. Once again, explanations and corrective proceedures quickly started to appear in the literature.

It soon became apparent that the load characteristics of an HVDC link generally display negative damping at a variety of subsynchronous frequencies. Under the appropriate conditions, the negative damping of an HVDC link can cause the entire system to go unstable, with the generator shaft oscillations at one of its natural frequencies.

It seems very intuitive that the best way to control subsynchronous torsional interactions (SSTI) between an HVDC link and a turbine–generator is to carefully design the HVDC link and/or power plant in such a manner that the torsional modes are not excited in the first place. In other words,

the torsional modes should be positively damped in an optimally designed system. (Such a design approach is discussed by R. J. Piwko, et al. [7]) For a whole host of reasons, however, an optimal design is not always possible. In such cases supplementary subsynchronous damping controllers (SSDC) can be added to the HVDC controls in order to maintain stability.

Generally, SSDC's require an input which reflects the generator speed deviation or the generator's instantaneous position [8]. This information is often measured directly from sensors located on the generator shaft.

There are, however, two major problems associated with such an approach. First, the generator shaft might not be directly accessible (due to shaft elasticity, sensors must be mounted directly at the generator), and a critical control input variable is lost. Second, even if the shaft information is available at the power plant, there is still the problem of forwarding these data to the SSDC located at the HVDC converter station which might be several hundred kilometers away.

1.3 Problem

The determination of the generator speed deviation can often prove difficult, especially at large distances from the generating station. This speed deviation, however, also causes a distortion of the generator's internal voltage and output current. Since a unique relation exists between the speed deviation and the voltage (and current) distortion, development of an appropriate analysis technique has the potential to eliminate the need for direct speed measurement. The intent of this thesis is to develop such an analysis technique and test its validity and accuracy using EMTDC simulation for passive, as well as active, HVDC load configurations.

Chapter 2

The Electro–Mechanical Machine Model

2 .1 Introduction

In order for the effects of subsynchronous torsional interactions to be studied, a synchronous machine model must be employed which accurately represents the electro–mechanical interactions that occur in a turbine–generator. The electrical properties of the machine are naturally modelled with the help of Park's Transform [9], while the mechanical system is directly modelled by a set of differential equations.

2 .2 The D–Q Axis Machine Model

The field and armature windings of a three phase synchronous machine are all magnetically coupled. Due to the generator action of the machine, its mathematical model consists of at least four mutually dependant differential equations.

In order to solve this system of equations, R. H. Park suggested a transformation matrix which could be used in order to decouple the equations. Park's Transform converts the three phase A, B, C, 60 hertz quantities into d–q–0 DC quantities. The transform and inverse transform matricies are given below.

$$T(\theta) = \frac{2}{3}\begin{bmatrix} \cos(\theta) & \cos(\theta - 2\pi/3) & \cos(\theta - 4\pi/3) \\ \sin(\theta) & \sin(\theta - 2\pi/3) & \sin(\theta - 4\pi/3) \\ 1/2 & 1/2 & 1/2 \end{bmatrix} \tag{2.1}$$

$$T^{-1}(\theta) = \begin{bmatrix} \cos(\theta) & \sin(\theta) & 1 \\ \cos(\theta - 2\pi/3) & \sin(\theta - 2\pi/3) & 1 \\ \cos(\theta - 4\pi/3) & \sin(\theta - 4\pi/3) & 1 \end{bmatrix} \tag{2.2}$$

where θ = the rotor position measured from the d–axis of the machine.

All three–phase and d–q–axis quantities are related through this transformation. The values i_a, i_b and i_c are the phase currents, and i_d, i_q and i_0 are the transformed d, q, and 0–axis currents. (Similar notation is used for the voltages, v and the fluxes, Ψ.)

$$\begin{bmatrix} i_d \\ i_q \\ i_0 \end{bmatrix} = T(\theta)\begin{bmatrix} i_a \\ i_b \\ i_c \end{bmatrix} \qquad \begin{bmatrix} v_d \\ v_q \\ v_0 \end{bmatrix} = T(\theta)\begin{bmatrix} v_a \\ v_b \\ v_c \end{bmatrix} \qquad \begin{bmatrix} \Psi_d \\ \Psi_q \\ \Psi_0 \end{bmatrix} = T(\theta)\begin{bmatrix} \Psi_a \\ \Psi_b \\ \Psi_c \end{bmatrix} \tag{2.3}$$

Since Park's Transform and the rather lengthy application of his transform are very well known, only a brief summary of the resulting machine equations in the new d–q axis reference frame is given. A very complete discussion of the transform can be found in a variety of books [9][10][11]. In the new reference frame, it can be shown that the fluxes Ψ and currents i are now very simply related:

$$\Psi_d = L_d\ i_d + L_{md}\ i_f' \tag{2.4}$$

$$\Psi_q = L_q\ i_q \tag{2.5}$$

$$\Psi_0 = L_0\ i_0 \tag{2.6}$$

$$\Psi_f' = L_{md}\ i_d + L_{ff}\ i_f' \tag{2.7}$$

where L_d is the self–inductance of the d–axis winding

L_q is the self–inductance of the q–axis winding

L_0 is the zero–sequency inductance

L_{md} is the d–axis magnitizing (or mutual) inductance

L_{mq} is the q–axis magnitizing (or mutual) inductance

L_{ff} is the self–inductance of the field winding

i_f' is the reflected field current seen from the stator side

and Ψ_f' is the reflected field flux seen from the stator side

As can be seen the d–q–0 flux equations are all independent of one another. It can also be seen that the field is coupled only to the d axis.

Application of the Park Transform also yields the following set of differential equations relating the voltages to the fluxes and currents:

$$v_d - i_d\ R_a = \omega \Psi_q + \frac{d\Psi_d}{dt} \qquad (2.8)$$

$$v_q - i_q\ R_a = -\omega \Psi_d + \frac{d\Psi_q}{dt} \qquad (2.9)$$

$$v_0 - i_0\ R_0 = \frac{d\Psi_0}{dt} \qquad (2.10)$$

$$v_f' - i_f'\ R_f = \frac{d\Psi_f'}{dt} \qquad (2.11)$$

It is very important to note all quantities in the d–q–0 reference frame are constant in the steady state. This means that in the steady state all the differentials are zero. It should also be realized that $v_0 = i_0 = \Psi_0 = 0$ under all balanced load conditions. Since all work in this thesis is based on the assumption of a balanced load, the zero sequence equations will be completely omitted in future discussions.

2 .3 Calculation of the Steady State Voltage

When a synchronous machine is running in the steady state, a constant (dc) field voltage is required. This field voltage comes from the exciter which may be constructed in a variety of ways. Some possible construction styles include dc machines, ac machines with some rectification, or completely electronic devices. In most studies of SSR, however, the modelling of the excitation system is not required [12] . Also since the different types of exciters have such very different properties, it is hardly worth the inclusion of an excitation system unless the specific effects of one particular exciter are to be examined in great detail. Therefore, for the purposes of this thesis it will suffice to simply model the entire excitation system by a constant field voltage with the appropriate magnitude to yield 1.0 p.u. terminal voltage for the given load under study.

Use of this approach, however, requires the calculation of the exact excitation voltage in advance. This excitation voltage is determined using the D–Q axis machine equations in the steady state.

The phasor diagram for a salient pole synchronous machine is given in Figure 2 .1 . The standard convention for normalizing the field voltage is to set the voltage base to be equal to the voltage required to supply 1.0 p.u. terminal voltage on the machine under a no load condition (this normalized field quantity is referred to as V_f') Using this convention, the terminal voltage of the machine is given by:

$$V_t = V_f' - R_a I_a - jX_d I_d - jX_q I_q \qquad (2.12)$$

where R_a, the armature resistance, is small and will be neglected.

$X_d = j\omega L_d$ and is the d–axis reactance

$X_q = j\omega L_q$ and is the q–axis reactance

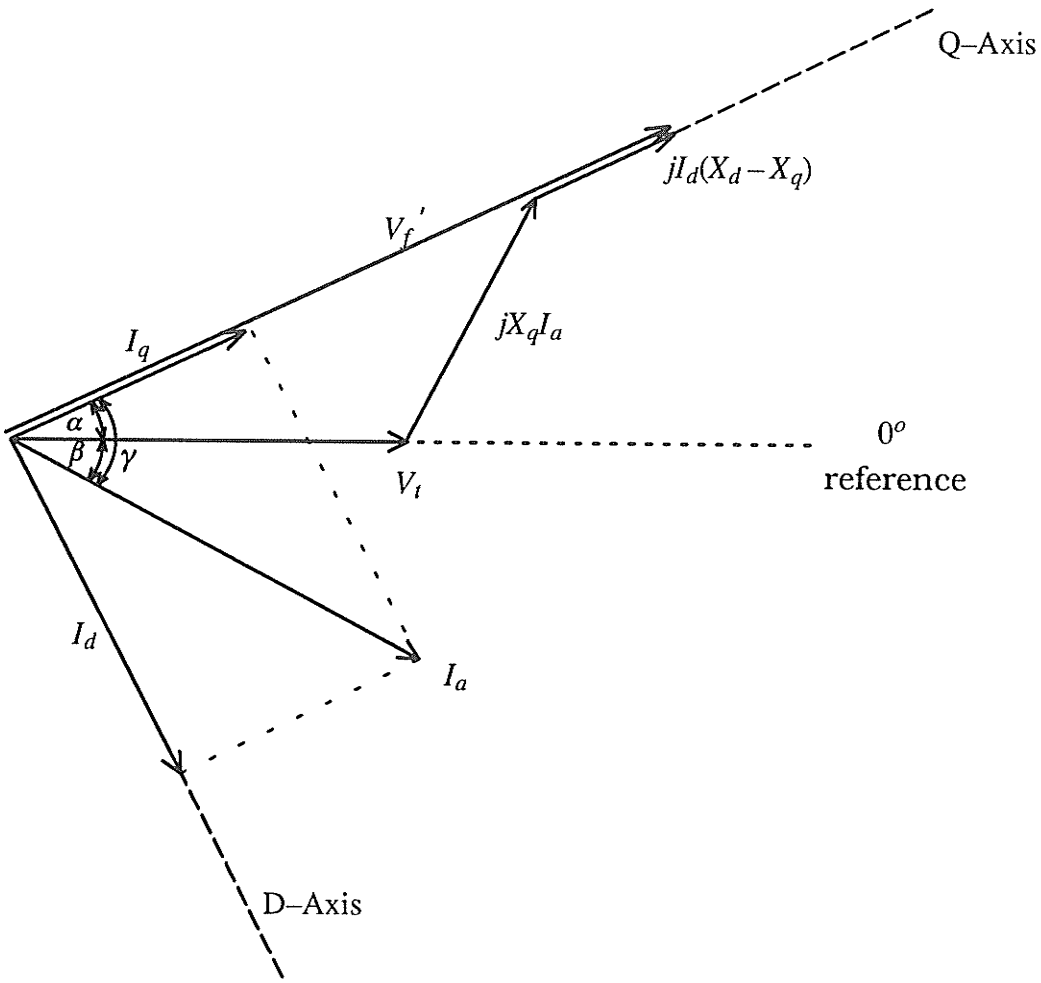

Figure 2 .1 : Phasor Diagram of a Salient Pole Synchronous Machine

Manipulation of equation 2 .12 by adding and subtracting the quantity jX_qI_d yields:

$$V_f' = V_t + jX_q(I_d + I_q) + jI_d(X_d - X_q) \quad .$$

(2 .13)

From the phasor diagram, however, it is apparent the $I_a = I_d + I_q$ therefore equation 2 .13 can be simplified to:

$$V_f' = V_t + jX_qI_a + j(X_d - X_q)I_d \quad .$$

(2 .14)

Since the vector sum of V_t and jX_qI_a lies along the quadrature axis (as can be seen in the phasor diagram) the angles α , β and γ can be easily determined.

$$\alpha = \angle(V_t + jX_qI_a) - \angle(V_t) \tag{2.15}$$

$$\beta = \angle(V_t) - \angle(I_a) \tag{2.16}$$

$$\gamma = \alpha + \beta \tag{2.17}$$

Finally this allows for the calculation of I_d.

$$I_d = I_a \sin\gamma \tag{2.18}$$

Hence the field voltage is now uniquely defined as a function of the load currents, terminal voltage and the machine parameters [9].

2 .4 The Multimass Machine Model

A turbine–generator system generally consists of several turbines and one generator mounted on a single continuous shaft. In the steady state, each unit moves at exactly the base speed of the machine without any deviations.

Figure 2 .2 shows a typical lumped element spring–mass turbine–generator model. For the purposes of this discussion three masses will be used, however, the expansion of the theory to four or more masses should be self–evident.

The linear model shown in this figure accurately represents the real system as long as the shaft is not stressed beyond its elastic limit. Certainly

for the purposes of this thesis it is reasonable to assume that the system will be operating within its linear range.

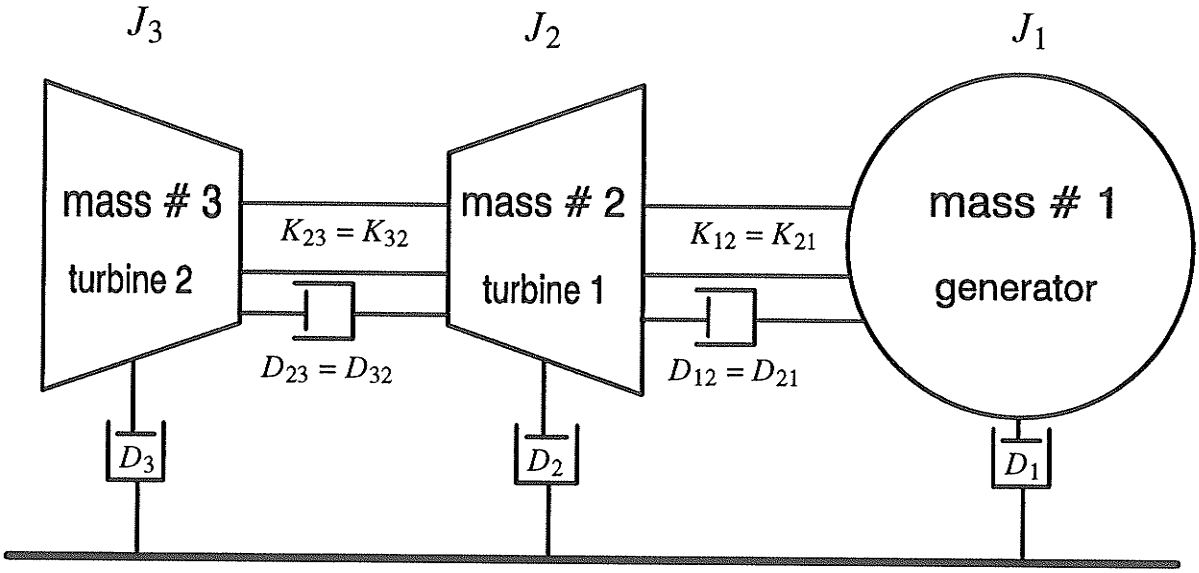

Figure 2 .2 : Lumped Element Spring-Mass Turbine-Generator Model.

Such a lumped element model is definitely not unique to turbine-generators and the equations describing the system are readily found in most books dealing with system modelling and control [13][14]. For convenience, though, these equations are stated without derivation below.

$$T_1 = J_1\frac{d\omega_1}{dt} + D_1\omega_1 + D_{12}(\omega_1 - \omega_2) + K_{12}(\theta_1 - \theta_2)$$

(2 .19)

$$T_2 = J_2\frac{d\omega_2}{dt} + D_2\omega_2 + D_{21}(\omega_2 - \omega_1) + D_{23}(\omega_2 - \omega_3) + K_{21}(\theta_2 - \theta_1) + K_{23}(\theta_2 - \theta_{3)}$$

(2 .20)

$$T_3 = J_3\frac{d\omega_3}{dt} + D_3\omega_3 + D_{32}(\omega_3 - \omega_2) + K_{32}(\theta_3 - \theta_2)$$

(2 .21)

where

T_i = the torque on mass i

J_i = the inertia of mass i

ω_i = the angular velocity of mass i

θ_i = the angular position of mass i

D_i = the self–damping of mass i

D_{ij} = the damping between masses i and j

K_{ij} = the spring constant between masses i and j

$D_{ij} = D_{ji}$

$K_{ij} = K_{ji}$

and

$$\omega_i = \frac{d\theta_i}{dt} \quad .$$

(2 .22)

Equation 2 .19 describes the motion of the generator. T_1 is therefore the electrical braking torque of the generator while T_2 and T_3 are the mechanical accelerating torques of the two turbines.

In large turbine–generator units all mechanical losses are minimized in order to obtain optimal efficiency. This results in extremely small self–damping coefficients. Also, due to the nearly ideal spring behaviour of the turbine–generator shaft, the damping between masses is also very small. These two facts permit the multimass model equations to be greatly simplified by assuming that the self damping and the intermass damping are both negligible, i.e.

$$D_i = 0$$

$$D_{ij} = 0$$

$$D_{ji} = 0 \ .$$

The simplified equations are:

$$T_1 = J_1 \frac{d\omega_1}{dt} + K_{12}(\theta_1 - \theta_2)$$

(2 .23)

$$T_2 = J_2 \frac{d\omega_2}{dt} + K_{21}(\theta_2 - \theta_1) + K_{23}(\theta_2 - \theta_3)$$

(2 .24)

$$T_3 = J_3 \frac{d\omega_3}{dt} + K_{32}(\theta_3 - \theta_2) \quad .$$

(2 .25)

A slightly more accurate system representation could be obtained by including all damping terms, assuming they are all known (which is generally not the case anyway). However, it is important to realize that the approximation is a very conservative one, because there will always be slightly more system damping than predicted by this model.

2 .5 The Theory of the Modal Model

The matrix solution of a multimass machine model can be carried out in various ways. If, however, damping terms are neglected, then a particularly effective "modal" approach can be used [15]. (Some approximate procedures for using a modal approach in a sytem with damping have been developed [12], but they generally introduce an unnecessary degree of complexity.) Fortunately, it is already known that the damping terms in the turbine–generator model are extremely small and that neglecting these terms will not introduce any significant errors.

In order to find the natural oscillating frequencies, the external torques in the system are set to zero. The equations 2 .23 through 2 .25 of the previous section can then be rewritten as:

$$0 = J_1 \frac{d\omega_1}{dt} + K_{12}(\theta_1 - \theta_2) \qquad (2.26)$$

$$0 = J_2 \frac{d\omega_2}{dt} + K_{21}(\theta_2 - \theta_1) + K_{23}(\theta_2 - \theta_3) \qquad (2.27)$$

$$0 = J_3 \frac{d\omega_3}{dt} + K_{32}(\theta_3 - \theta_2) \quad , \qquad (2.28)$$

where of course,

$$\omega_1 = \frac{d\theta_1}{dt} \qquad \omega_2 = \frac{d\theta_2}{dt} \qquad \omega_3 = \frac{d\theta_3}{dt} \quad .$$

These six equations can now be condensed to three second order differential equations (with no single derivatives of position at all).

$$0 = J_1 \frac{d^2\theta_1}{dt^2} + K_{12}\theta_1 - K_{12}\theta_2 \qquad (2.29)$$

$$0 = J_2 \frac{d^2\theta_2}{dt^2} - K_{21}\theta_1 + (K_{21} + K_{23})\theta_2 - K_{23}\theta_3 \qquad (2.30)$$

$$0 = J_3 \frac{d^2\theta_3}{dt^2} + K_{32}\theta_2 - K_{32}\theta_3 \quad , \qquad (2.31)$$

or in matrix form

$$\begin{bmatrix} J_1 & 0 & 0 \\ 0 & J_2 & 0 \\ 0 & 0 & J_3 \end{bmatrix} \frac{d^2}{dt^2} \begin{bmatrix} \theta_1 \\ \theta_2 \\ \theta_3 \end{bmatrix} + \begin{bmatrix} K_{12} & -K_{12} & 0 \\ -K_{21} & K_{21} + K_{23} & -K_{23} \\ 0 & -K_{23} & K_{32} \end{bmatrix} \begin{bmatrix} \theta_1 \\ \theta_2 \\ \theta_3 \end{bmatrix} = 0 \quad . \qquad (2.32)$$

In general, this matrix equation can be simply expressed as

$$[J]\frac{d^2\theta}{dt^2} + [K]\theta = 0 \quad .$$

(2 .33)

However, in this case it is much more useful to let $[N]^2 = [J]$ and write

$$[N]^2\frac{d^2\theta}{dt^2} + [K]\theta = 0 \quad .$$

(2 .34)

Applying the change of variables $y = [N]\theta$ to equation 2 .34 yields

$$[N]\frac{d^2y}{dt^2} + [K][N]^{-1}y = 0$$

(2 .35)

or

$$\frac{d^2y}{dt^2} + [N]^{-1}[K][N]^{-1}y = 0 \quad .$$

(2 .36)

If matrix [C] is now chosen so that it diagonalizes the matrix $[N]^{-1}[K][N]^{-1}$,

i.e.

$$[C]\left\{[N]^{-1}[K][N]^{-1}\right\}[C]^{-1} = [\lambda] \quad ,$$

(2 .37)

then a final change of variables $y = [C]z$ will completely decouple the system of second order differential equations. Thus equation 2 .36 becomes:

$$[C]\frac{d^2z}{dt^2} + \left\{[N]^{-1}[K][N]^{-1}\right\}[C]\ z = 0 \qquad (2.38)$$

$$\frac{d^2z}{dt^2} + [C]^{-1}\left\{[N]^{-1}[K][N]^{-1}\right\}[C]\ z = 0 \qquad (2.39)$$

which (due to equation 2 .37) is identical to

$$\frac{d^2z}{dt^2} + [\lambda]\ z = 0 \ . \qquad (2.40)$$

Since this system is now decoupled, we can simply write

$$\frac{d^2z_i}{dt^2} + \lambda_i\ z_i = 0 \ , \qquad (2.41)$$

which has the general solutions of

$$z_i = A_i t + B \qquad \text{for } \lambda_i = 0$$

$$z_i = A_i \sin(\omega_{ni} t + \phi_i) \qquad \text{for } \lambda_i > 0$$

where $\omega_{ni} = \sqrt{\lambda_i}$. (2.42)

Hence the eigenvalues λ_i , $i = 1, \ldots n$ are simply the eigenvalues of $[N]^{-1}[K][N]^{-1}$ as shown in equation 2 .37 and the transformation matrix between the z and θ reference frames can be found from the two substitutions that were performed.

$$\theta = [N]^{-1}y = [N]^{-1}[C]\ z \qquad (2.43)$$

2 .6 The Calculation of Normalized Mode Shapes

The fundamental advantage of using a modal approach is its ability to determine the normalized mode shapes of a turbine–generator. When a power system is subject to any sort of disturbance, the multimass turbine–generator unit begins to oscillate at its resonant frequencies (given by $\omega_{ni} = \sqrt{\lambda_i}$ in the previous section). Due to the variety of inertia and spring constant values, however, each mass oscillates at each frequency with its own amplitude. Although the amplitudes vary from mass to resonant frequency there is a "mode shape" which gives the ratios of the oscillation amplitudes between all masses for that one specific frequency. Since this mode shape is indeed frequency dependent one mode shape exists for each resonant frequency. The calculation procedure required to determine the mode shapes of the three mass turbine–generator system shown in Figure 2 .2 will now be presented. Since this system has 3 masses, 3 eigenvalues will exist. The first eigenvalue always turns out to be zero because of the nature of the matrix equation. (This is also physically reasonable because the entire mass assembly must rotate at synchronous frequency and this corresponds to $z_1 = \omega_o t$ in equation 2 .45) Therefore 3 modes result, but only the modes associated with the 2 non–zero eigenvalues represent resonant oscillations.

The eigenvalues will therefore be:

$$\lambda_1 = 0$$
$$\lambda_2 = \omega_{n2}^2$$
$$\lambda_3 = \omega_{n3}^2 \qquad (2.44)$$

and the modes of oscillation will be:

$$z_1 = A_1 t + \phi_1$$

$$z_2 = A_2 \sin(\omega_{n2} t + \phi_2)$$

$$z_3 = A_3 \sin(\omega_{n3} t + \phi_3) \qquad (2.45)$$

where once again it can be seen that the first mode does not actually oscillate.

The angular position of each mass can now be found by applying the transform given in equation 2.43 to the equations 2.45.

$$\begin{bmatrix} \theta_1 \\ \theta_2 \\ \theta_3 \end{bmatrix} = [N]^{-1}[C] \begin{bmatrix} z_1 \\ z_2 \\ z_3 \end{bmatrix} \qquad (2.46)$$

To simplify this equation, let $[R] = [N]^{-1}[C]$ to give:

$$\begin{bmatrix} \theta_1 \\ \theta_2 \\ \theta_3 \end{bmatrix} = \begin{bmatrix} r_{11} & r_{12} & r_{13} \\ r_{21} & r_{22} & r_{23} \\ r_{31} & r_{32} & r_{33} \end{bmatrix} \begin{bmatrix} A_1 t + \phi_1 \\ A_2 \sin(\omega_{n2} t + \phi_2) \\ A_3 \sin(\omega_{n3} t + \phi_3) \end{bmatrix} \qquad (2.47)$$

or, setting $\phi_1 = 0$ as a chosen frame of reference and collecting terms:

$$\begin{bmatrix} \theta_1 \\ \theta_2 \\ \theta_3 \end{bmatrix} = \begin{bmatrix} r_{11}A_1 & r_{12}A_2 & r_{13}A_3 \\ r_{21}A_1 & r_{22}A_2 & r_{23}A_3 \\ r_{31}A_1 & r_{32}A_2 & r_{33}A_3 \end{bmatrix} \begin{bmatrix} t \\ \sin(\omega_{n2} t + \phi_2) \\ \sin(\omega_{n3} t + \phi_3) \end{bmatrix} \qquad (2.48)$$

In the above equation the quantity θ_1 gives the angular position of the generator. All oscillating amplitudes can now be normalized with respect to the generator oscillating amplitudes. Since all three masses are rotating

at the same base speed, it can be shown that $r_{11} = r_{21} = r_{31}$.

$$\begin{bmatrix} \theta_{1_n} \\ \theta_{2_n} \\ \theta_{3_n} \end{bmatrix} = \begin{bmatrix} 1 & 1 & 1 \\ 1 & r_{22}/r_{12} & r_{23}/r_{13} \\ 1 & r_{32}/r_{12} & r_{33}/r_{13} \end{bmatrix} \begin{bmatrix} t \\ \sin(\omega_{n2}t + \phi_2) \\ \sin(\omega_{n3}t + \phi_3) \end{bmatrix} \tag{2.49}$$

or simply,

$$\theta_n = [R_n]\ z_n \tag{2.50}$$

The mode shapes associate with the modes of oscillation are given by the columns in the matrix $[R_n]$. The three mode shapes are given below along with their corresponding resonant frequencies. Mode 1 is often referred to as the rigid–body mode since it corresponds to all three masses moving together. In a normal system they would move together at a speed of ω_o .

Table 2 .1 : Normalized Mode Shapes of a Three Mass Turbine–Generator

mass	Mode 1 ω_{n1} = 0 rad/s	Mode 2 $\omega_{n2} = \sqrt{\lambda_2}$ rad/s	Mode 3 $\omega_{n3} = \sqrt{\lambda_3}$ rad/s
generator	1	1	1
turbine 1	1	r_{22} / r_{12}	r_{23} / r_{13}
turbine 2	1	r_{32} / r_{12}	r_{33} / r_{13}

2 .7 The Machine Model Under Study

For the purposes of this thesis, one particular turbine–generator unit will be employed. The unit to be used was somewhat arbitrarily selected to be a 588 MVA machine produced by ABB. The primary motivation behind choosing this unit was the ready availability of all necessary turbine–generator data.

Figure 2 .3 shows a reduced lumped element spring–mass model of the turbine–generator under study.

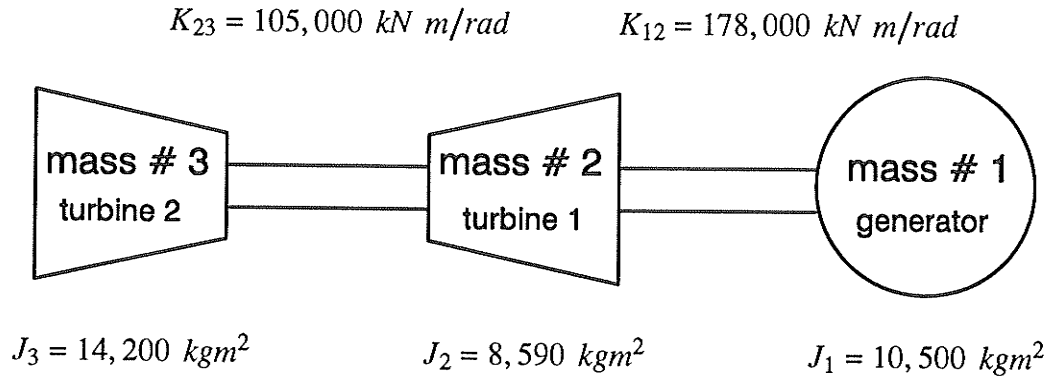

Figure 2 .3 : The Turbine–Generator under Study.

Modal analysis of this system can easily be carried out using most pre–packaged programs equipped to solve for eigenvalues and eigenvectors. Appendix A gives the Mathcad 3.0 routine required to solve for the resonant frequencies and normalized mode shapes of the multimass system shown in Figure 2 .3 . The results of this analysis are summarized below.

The resonant frequencies of the system are:

$$\omega_{n1} = 0 \ \ rad/sec \qquad f_{n1} = 0 \ \ hz$$

$$\omega_{n2} = 104.4 \ \ rad/sec \qquad f_{n2} = 16.61 \ \ hz$$

$$\omega_{n3} = 211.2 \ \ rad/sec \qquad f_{n3} = 33.61 \ \ hz$$

The mode shapes are given in Table 2 .2 .

Table 2 .2 : Mode Shapes of the Turbine–Generator under Study

mass	Mode 1 f_{n1} = 0 hz	Mode 2 f_{n2} = 16.61 hz	Mode 3 f_{n3} = 33.61 hz
generator	1	1	1
turbine 1	1	– 0.6852	1.553
turbine 2	1	– 0.0896	–3.458

These specific mode shapes will later be required to determine the oscillation amplitudes on turbines 1 and 2 given a known oscillation of the generator.

Chapter 3

Determination of Shaft Oscillations from Generator Terminal Quantities

3 .1 Introduction

The modal analysis presented in Sections 2.5 through 2.7 proves extremely valuable in determining the oscillating amplitudes of all turbines given the generator's amplitudes of oscillation. These generator quantities can be determined from the generator's terminal voltage and/or current waveforms provided that an overly complex machine model is not employed.

3 .2 Approximations to the Electrical Machine Model

In order to facilitate the development of an analytic procedure which is capable of determining generator shaft oscillations from terminal quantities, the following assumptions and approximations are made:

1. The machine is assumed to be a linear device; or at very least to have a linear small signal response.
2. It is assumed that the machine is accurately represented by the D–Q Axis model. (i.e. use of Park's Transform itself requires certain approximations to be made [9] and these are simply accepted as a consequence of using his transform.)
3. The effects of damper windings are ignored.
4. The armature resistance of the synchronous generator is considered negligible and its effect is ignored. (This assumption is only required under load conditions.)

5. It is assumed that the machine is basically operating in the steady state and that any disturbances to the system only cause slight perturbations to the steady state quantities.
6. The machine is always operating under balanced load conditions.

Certain further approximations will be required throughout the development of the analytic procedure and they will be discussed as they are made.

3 .3 The Electric Machine under No Load

Under a no load condition, the synchronous generator machine equations can be greatly simplified. Since under no load the phase currents are all zero, the d–q axis currents are also zero. Setting $i_d = 0$ and $i_q = 0$ in the flux equations of section 2.2 (equations 2 .4 to 2 .7) yields

$$\Psi_d = L_{md}\, i_f' \qquad (3.1)$$

$$\Psi_q = 0 \qquad (3.2)$$

$$\Psi_f' = L_{ff}\, i_f' \quad . \qquad (3.3)$$

Also, if steady state operation is assumed, all differentials in the voltage equations of section 2.2 are zero. (This is because the d–q axis quantities are DC.) Thus equations 2 .8 , 2 .9 and 2 .11 are simplified to:

$$v_d = \omega \Psi_q \qquad (3.4)$$

$$v_q = -\omega \Psi_d \qquad (3.5)$$

$$v_f' = R_f\, i_f' \quad , \qquad (3.6)$$

From equation 3 .6 it can be seen that the field current is constant in the steady state and given by $i_f' = v_f'/R_f$. This results in the d–axis flux

of equation 3.1 being constant as well. Thus, for simplicity, equation 3.1 is rewritten as follows:

$$\Psi_d = L_{md}\, i_f{}' = \Psi_{do} \quad . \tag{3.7}$$

Substituting the necessary values of flux into the d and q axis voltage equations yields

$$v_d = 0 \tag{3.8}$$

$$v_q = -\omega \Psi_d \quad . \tag{3.9}$$

With the application of Park's Transform, these new d and q axis voltage equations can be used to determine the three phase terminal voltage:

$$\begin{bmatrix} v_d \\ v_q \\ v_0 \end{bmatrix} = \mathrm{T}(\theta) \begin{bmatrix} v_a \\ v_b \\ v_c \end{bmatrix} \quad . \tag{3.10}$$

This yields a phase A voltage of

$$v_a = v_q \sin\theta \tag{3.11}$$

or

$$v_a = -\omega \Psi_{do} \sin\theta \quad , \tag{3.12}$$

while the B and C phase voltages are simply shifted by plus/minus 120 degrees.

In order to proceed further, an expression for θ and ω, the generator's position and speed, must be developed. Normally the mechanical angular position of the generator shaft in a two pole

synchronous machine is given by

$$\theta = \omega_o t \qquad (3.13)$$

where ω_o = the electrical base speed (equal to the mechanical base speed for a two–pole machine).

If, however, the generator is subject to a resonant oscillation (as discussed in Chapter 2) with amplitude β and frequency ω_x then the equation for the generator's shaft position becomes

$$\theta = \omega_o t + \beta \sin \omega_x t \qquad (3.14)$$

where the possibility of a phase shift in the resonant oscillation is ignored, since it is of no consequence in the following analysis.

Given an expression for the shaft position, the shaft speed can be easily determined from the relation:

$$\omega = \frac{d\theta}{dt} \quad . \qquad (3.15)$$

Hence,

$$\omega = \omega_o + \beta\omega_x \cos \omega_x t \quad . \qquad (3.16)$$

Now returning to the phase A voltage equation 3.12, the values of θ and ω given in equations 3.14 and 3.16 can be substituted to yield:

$$v_a = -(\omega_o + \beta\omega_x \cos \omega_x t)\ \Psi_{do} \sin(\omega_o t + \beta \sin \omega_x t) \quad . \qquad (3.17)$$

For small values of β (which will later be seen to be always the case)

the following approximation can be made:

$$\sin(\omega_o t + \beta \sin \omega_x t) \approx \sin \omega_o t + \beta \sin \omega_x t \cos \omega_o t \quad .$$

(3 .18)

Application of the trigonometric product identity on the last term of the above equation yields:

$$\beta \sin \omega_x t \cos \omega_o t = \frac{\beta}{2} \left\{ \sin[(\omega_x - \omega_o)t] + \sin[(\omega_x + \omega_o)t] \right\} \quad .$$

(3 .19)

Thus making the substitutions suggested in equations 3 .18 and 3 .19 yield a new equation for v_a.

$$v_a = -(\omega_o + \beta\omega_x \cos \omega_x t)\ \Psi_{do} \left\{ \sin \omega_o t + \frac{\beta}{2}[\sin((\omega_x - \omega_o)t) + \sin((\omega_x + \omega_o)t)] \right\} \quad .$$

(3 .20)

Expansion of equation 3 .20 yields:

$$v_a = -\Psi_{do} \left\{ \omega_o \sin \omega_o t + \frac{\beta\omega_o}{2}[\sin((\omega_o + \omega_x)t) - \sin((\omega_o - \omega_x)t)] \right.$$

$$\left. + \beta\omega_x \cos \omega_x t \sin \omega_o t + \frac{\beta^2\omega_x}{2} \cos \omega_x t [\sin((\omega_o + \omega_x)t) - \sin((\omega_o - \omega_x)t)] \right\} \quad .$$

(3 .21)

Once again the product terms in the above equation are eliminated using trigonometric identities.

$$\beta\omega_x \cos \omega_x t \sin \omega_o t \approx \frac{\beta\omega_x}{2} \left\{ \sin((\omega_o + \omega_x)t) + \sin((\omega_o - \omega_x)t) \right\}$$

(3 .22)

$$\frac{\beta^2\omega_x}{2} \cos \omega_x t [\sin((\omega_o + \omega_x)t) - \sin((\omega_o - \omega_x)t)] \approx \frac{\beta^2\omega_x}{4} [\sin((\omega_o + 2\omega_x)t) - \sin((\omega_o - 2\omega_x)t)]$$

(3 .23)

Replacing the product terms in equation 3 .21 with their equivalences given in equations 3 .22 and 3 .23 and simplifying yields:

$$v_a = -\Psi_{do}\left\{\omega_o \sin\omega_o t + \frac{\beta}{2}(\omega_o+\omega_x)\sin((\omega_o+\omega_x)t) - \frac{\beta}{2}(\omega_o-\omega_x)\sin((\omega_o-\omega_x)t)\right.$$

$$\left. + \frac{\beta^2\omega_x}{4}\sin((\omega_o+2\omega_x)t) - \frac{\beta^2\omega_x}{4}\sin((\omega_o-2\omega_x)t)\right\} . \qquad (3.24)$$

Since it has already been stated that β is small the above formula can be approximated by setting $\beta^2 = 0$.

$$v_a \approx -\Psi_{do}\left\{\omega_o \sin\omega_o t + \frac{\beta}{2}(\omega_o+\omega_x)\sin((\omega_o+\omega_x)t) - \frac{\beta}{2}(\omega_o-\omega_x)\sin((\omega_o-\omega_x)t)\right\} \qquad (3.25)$$

or if equation 3 .25 is normalized:

$$v_{a_n} = \sin\omega_o t + \frac{\beta}{2\omega_o}(\omega_o+\omega_x)\sin((\omega_o+\omega_x)t) - \frac{\beta}{2\omega_o}(\omega_o-\omega_x)\sin((\omega_o-\omega_x)t) \qquad (3.26)$$

Inspection of the above equation shows that the voltage waveform v_a has a component at the fundamental frequency ω_o, as well as two additional components; one at $\omega_o+\omega_x$ and one at $\omega_o-\omega_x$ (where, once again, ω_x is the frequency of the mechanical oscillation superimposed on the shaft speed). Finally, equation 3 .26 can be expressed graphically in terms of its Fourier spectrum as shown in Figure 3 .1 .

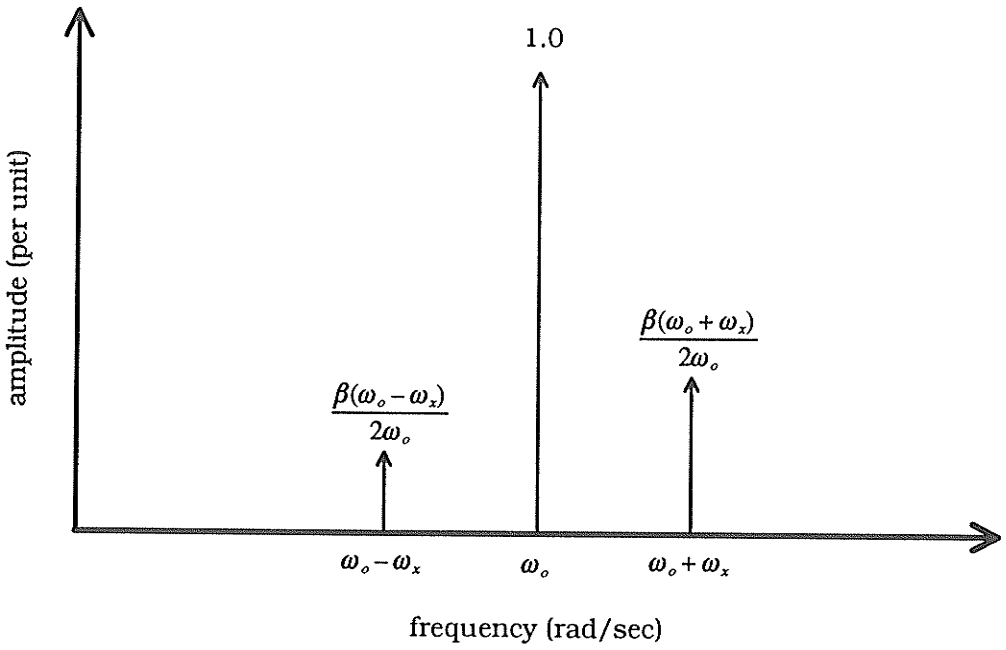

Figure 3 .1 : Expected Fourier Spectrum of the Terminal Voltage of a Generator whose Shaft is subject to a Mechanical Oscillation of Amplitude β and Frequency ω_x.

3 .4 The Electric Machine under a Passive Load

When the synchronous generator is driving a given load, the machine equations become somewhat more complex than described in the previous section. However, if the assumptions of section 3.1 are once again made, analysis of the machine subject to an arbitrary passive load becomes possible.

Since the machine is assumed to be stably operating in the steady state, all d–q axis currents will be constant (DC) values. The field current will also have a constant (DC) value. Therefore, all the machine fluxes will also be constant; this is symbolized by a subscript "o".

$$\Psi_d = L_d\ i_d + L_{md}\ i_f' \equiv \Psi_{do} \qquad (3.27)$$

$$\Psi_q = L_q \; i_q \equiv \Psi_{qo}$$

(3 .28)

$$\Psi_f{}' = L_{ff} \; i_f{}' + L_{md} \; i_d \equiv \Psi_{fo}{}'$$

(3 .29)

The d and q axis voltages are now given by

$$v_d = \omega \Psi_{qo}$$

(3 .30)

$$v_q = -\omega \Psi_{do} \quad .$$

(3 .31)

Once again the phase A terminal voltage of the machine is found by employing Park's Transform. It turns out to be

$$\begin{aligned} v_a &= v_d \cos\theta + v_q \sin\theta \\ &= \omega \Psi_{qo} \cos\theta - \omega_{gen} \Psi_{do} \sin\theta \quad . \end{aligned}$$

(3 .32)

A similar analysis is now carried out as presented in the previous section. Solution for the second term in this equation has already been given in equation 3 .25 and application of all the same simplifications to the first term yields a very similar result.

$$\begin{aligned} v_a \approx \Psi_{qo} &\left\{ \omega_o \cos\omega_o t + \frac{\beta}{2}(\omega_o + \omega_x)\cos((\omega_o + \omega_x)t) - \frac{\beta}{2}(\omega_o - \omega_x)\cos((\omega_o - \omega_x)t) \right\} \\ -\Psi_{do} &\left\{ \omega_o \sin\omega_o t + \frac{\beta}{2}(\omega_o + \omega_x)\sin((\omega_o + \omega_x)t) - \frac{\beta}{2}(\omega_o - \omega_x)\sin((\omega_o - \omega_x)t) \right\} \end{aligned}$$

(3 .33)

Normalization of this waveform, however, must be carried out in a much different manner than in the last section. First all terms of similar frequencies must be collected. This yields

$$v_a = \omega_o\left\{\Psi_{qo}\cos\omega_o t - \Psi_{do}\sin\omega_o t\right\}$$
$$+\frac{\beta}{2}(\omega_o+\omega_x)\left\{\Psi_{qo}\cos((\omega_o+\omega_x)t) - \Psi_{do}\sin((\omega_o+\omega_x)t)\right\}$$
$$-\frac{\beta}{2}(\omega_o-\omega_x)\left\{\Psi_{qo}\cos((\omega_o-\omega_x)t) - \Psi_{do}\sin((\omega_o-\omega_x)t)\right\} .$$

(3 .34)

The sines and cosines can now be combined using the phasor relation shown in equation 3 .35 ; this yields equation 3 .36 .

$$A\cos\omega t + B\sin\omega t = \sqrt{A^2+B^2}\ \sin(\omega t+\phi)$$

where $$\phi = \tan^{-1}\frac{A}{B}$$

(3 .35)

$$v_a = \omega_o\sqrt{\Psi_{qo}^2+\Psi_{do}^2}\ \sin(\omega_o t+\phi_1)$$
$$+\frac{\beta}{2}(\omega_o+\omega_x)\sqrt{\Psi_{qo}^2+\Psi_{do}^2}\ \sin((\omega_o+\omega_x)t+\phi_2)$$
$$+\frac{\beta}{2}(\omega_o-\omega_x)\sqrt{\Psi_{qo}^2+\Psi_{do}^2}\ \sin((\omega_o-\omega_x)t+\phi_3)$$

where $$\phi = \phi_1 = \phi_2 = \phi_3 = \tan^{-1}\left(\frac{-\Psi_{qo}}{\Psi_{do}}\right)$$

(3 .36)

Normalization of equation 3 .36 with respect to the fundamental can now be carried out. This yields the expression for v_a given in equation 3 .37 which corresponds to the normalized Fourier spectrum shown in Figure 3 .2 .

$$v_a = \sin(\omega_o t+\phi) + \frac{\beta}{2\omega_o}(\omega_o+\omega_x)\sin((\omega_o+\omega_x)t+\phi) + \frac{\beta}{2\omega_o}(\omega_o-\omega_x)sin((\omega_o-\omega_x)t+\phi)$$

(3 .37)

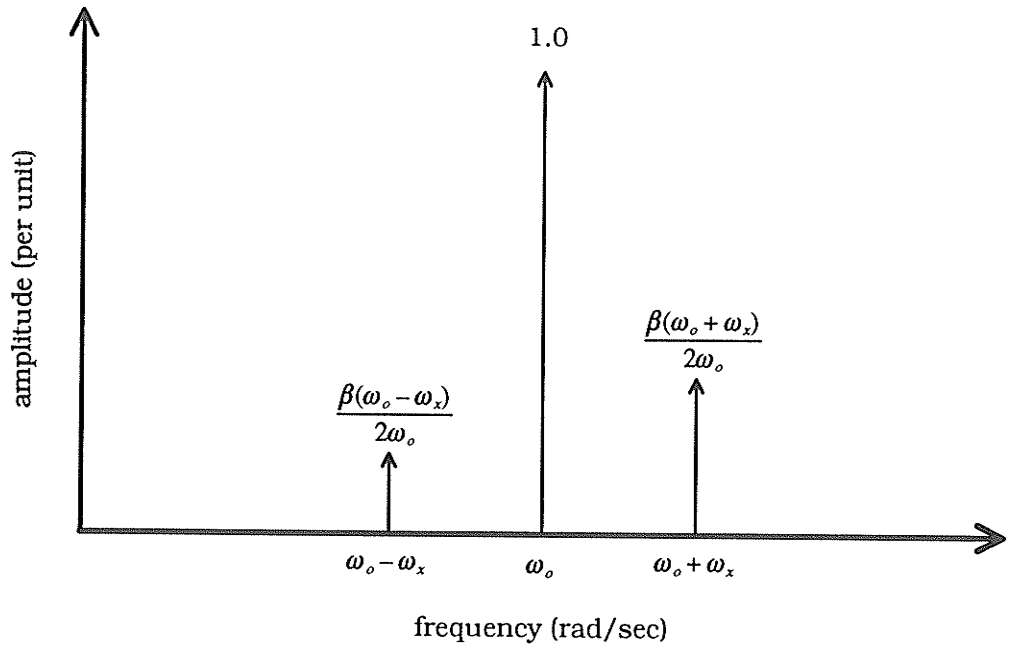

Figure 3 .2 : Expected Fourier Spectrum of the Terminal Voltage of a Generator whose Shaft is subject to a Mechanical Oscillation of Amplitude β and Frequency ω_x.

Comparing Figures 3 .1 and 3 .2 it can be seen that the normalized Fourier spectra of the generator's terminal voltage are completely independent of the load condition. This permits the theory to be used even in cases where no load information is available.

3 .5 Extension of the Theory for Multiple Resonances

The extension of the theory to accomodate two or more mechanical oscillating frequencies is quite trivial. If, for example, a three mass machine model were to be analyzed, two resonant frequencies would be found. If the amplitudes of these oscillations are β_1 and β_2 and their frequencies are ω_1 and ω_2 then the Fourier spectrum of the generator's terminal voltage will be as shown in Figure 3 .3 , where the generator shaft displacement and

speed are as given in equation 3 .38 .

$$\theta = \omega_o t + \beta_1 \sin \omega_1 t + \beta_2 \sin \omega_2 t \qquad (3.38)$$

$$\omega = \omega_o + \beta_1 \omega_1 \cos \omega_1 t + \beta_2 \omega_2 \cos \omega_2 t \qquad (3.39)$$

It should therefore be clear that if a spectrum analyzer were connected to the terminals of a generator that all values, ω_1 and ω_2, as well as β_1 and β_2 could be easily calculated and the instantaneous values of generator shaft speed and displacement (minus a possible off–set) would thus be known.

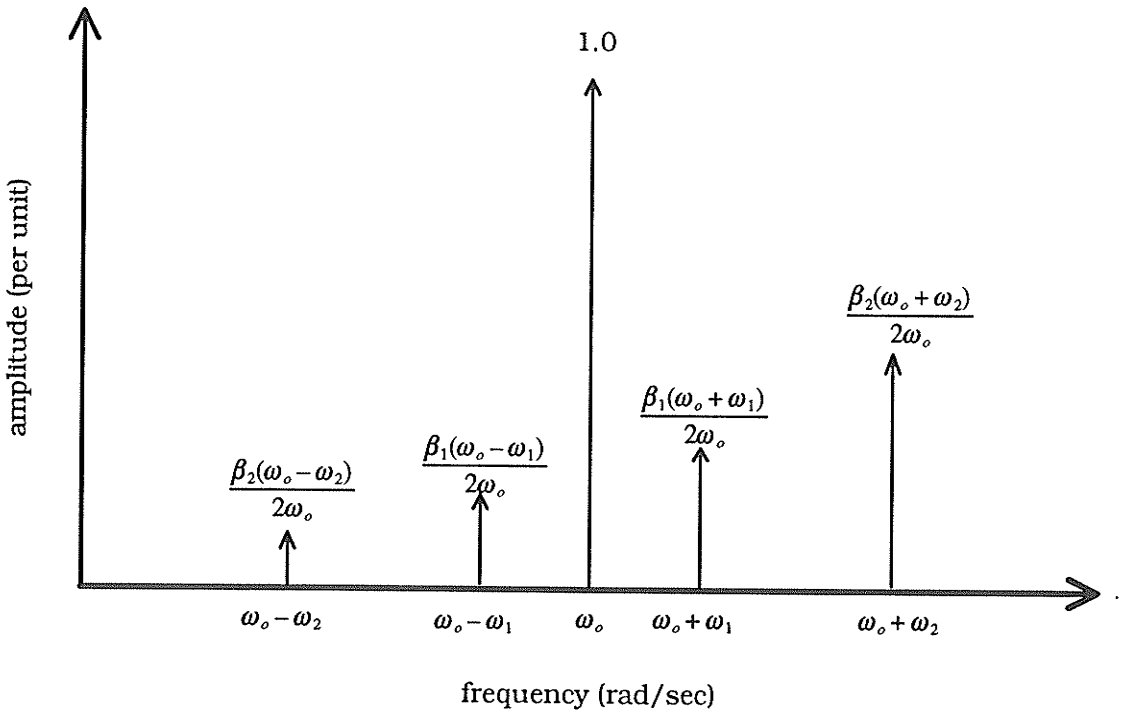

Figure 3 .3 : Expected Fourier Spectrum of the Terminal Voltage of a Three Mass Turbine–Generator

Combining the information on the generator's shaft speed and displacement with the mode shape theory of Chapter 2 (Sections 2.5 through 2.7) yields the speed and displacement of all turbines. Therefore,

all mechanical quantities of interest can be directly calculated from the normalized Fourier spectrum of a synchronous machine's terminal voltage.

Chapter 4

Verification of Theory by Simulation

4 .1 Introduction

The discussion presented so far has been based solely on theory. Also, in the theoretical development several approximations and assumptions had to be made. Although no gross oversimplifications to the model were required, the exact accuracy of the approach presented may seem somewhat questionable. Verification of the theory is therefore carried out by EMTDC simulation. Before this is done, however, it is important to realize some of the limitations inherent to the discrete time Fourier spectrum that will be applied.

4 .2 The Discrete Fourier Transform

As already stated, verification of the theory will be performed using the EMTDC simulation package. Since digital simulation is used, all subsequent analysis must be performed in the discrete time domain. This unfortunately means that all of the required Fourier spectra will have to be produced using the discrete Fourier Transform instead of the more desirable continuous Fourier Transform.

The common problem which arises when using the discrete Fourier Transform is aliasing. This occurs when the Nyquist sampling theorem is

not adhered to. Aliasing, however, is not a problem when working with EMTDC, because the output time step can be adjusted to yield any desired output frequency bandwidth.

The problem which does arise when performing a discrete Fourier Transform on an EMTDC output waveform stems from the sampled spectral output. In order to best describe this limitation it is beneficial to look at an example. Figure 4 .1 , on the next page, shows two curves, a 60 hz and a 33.7 hertz waveform with amplitudes of 1.0 and 0.25 respectively. The result of adding these two waveforms together is shown in Figure 4 .2 . (Figures 4 .1 and 4 .2 show only the first 0.08 seconds of the waveforms in question for the sake of graphical clarity.)

It is very important to minimize leakage noise [16] which results when the Fourier Transform is calculated over a non–integer number of periods. Since the 60 hz waveform has a much larger amplitude than the 33.7 hz waveform, the leakage noise is best minimized by truncating the combined signal at an integer number of 60 hz periods (i.e. at T_1, T_2, T_3, etc.). Figure 4 .3 shows the discrete Fourier Transform of the curve in Figure 4 .2 taken over T_3 seconds (with a sampling rate far exceeding the Nyquist rate).

The frequency axis must of course be scaled to represent hertz and this is shown by the secondary x–axis. It is important to notice that the separation between the bands in the spectrum is defined by Δf , given by

$$\Delta f = \frac{1}{T} \qquad (4.1)$$

where T = the interval of transformation in the time domain.

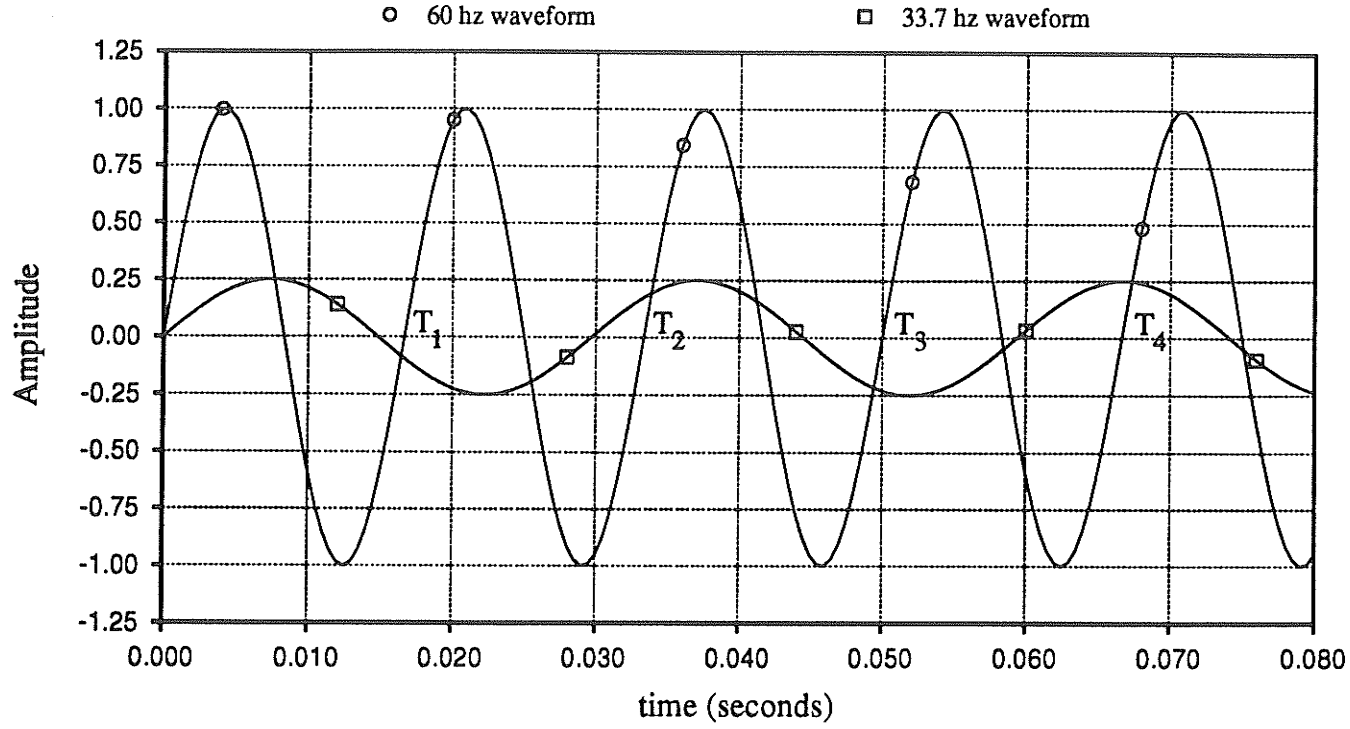

Figure 4.1: A 60 Hertz and 33.7 Hertz Waveform

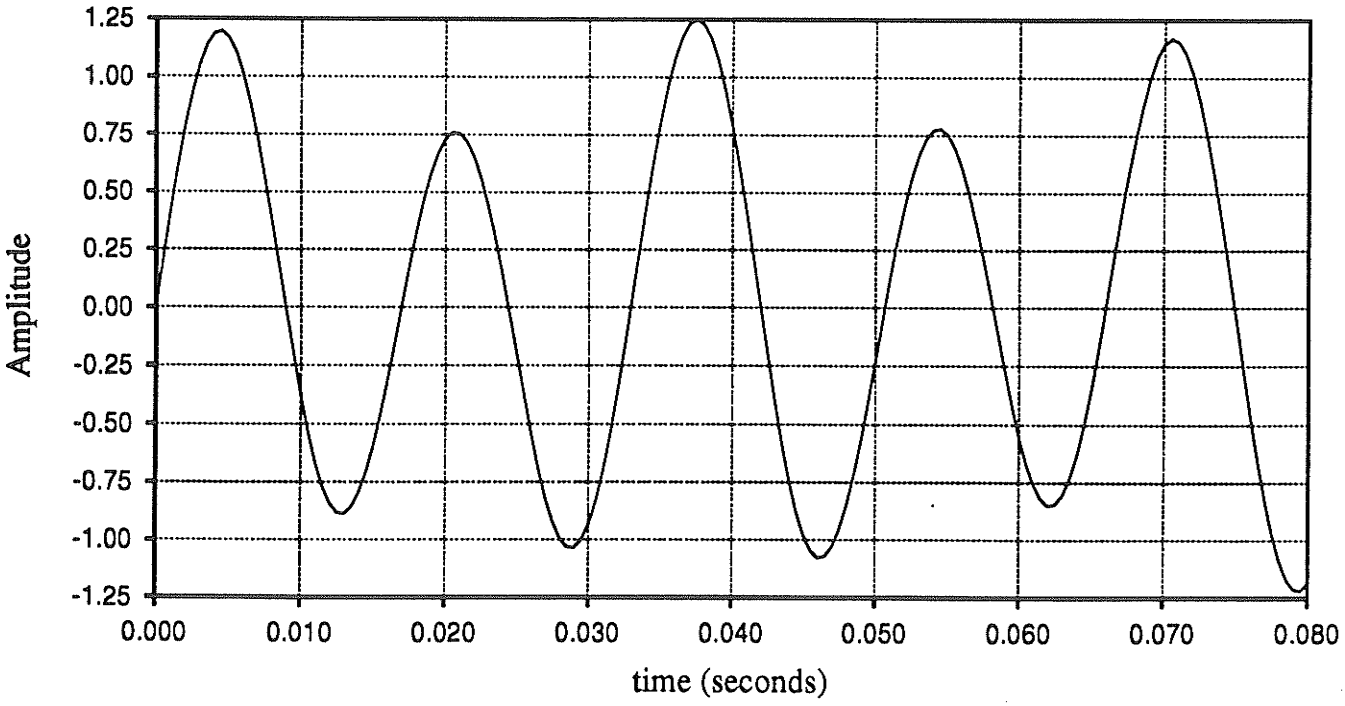

Figure 4.2: Sum of the Waveforms in Figure 4.1

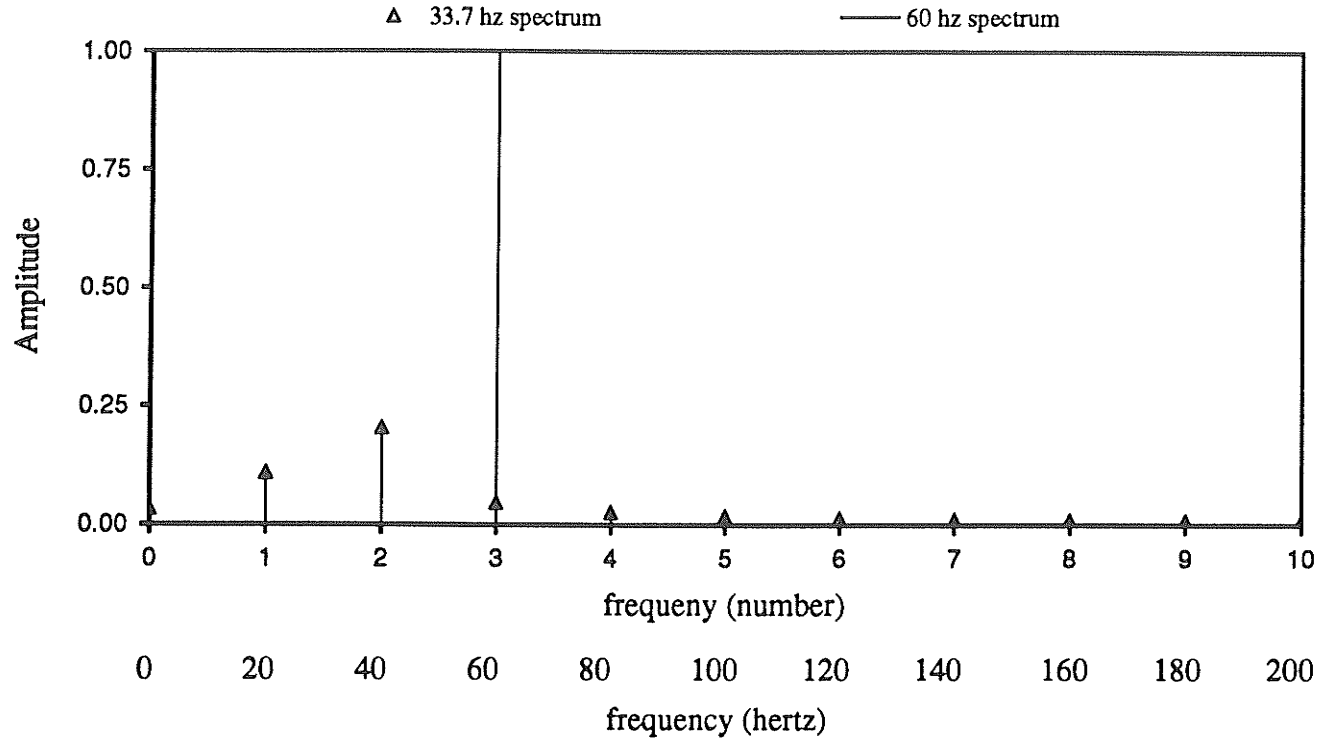

Figure 4.3: The Discrete Fourier Transform over a Time Interval of 0.05 Seconds

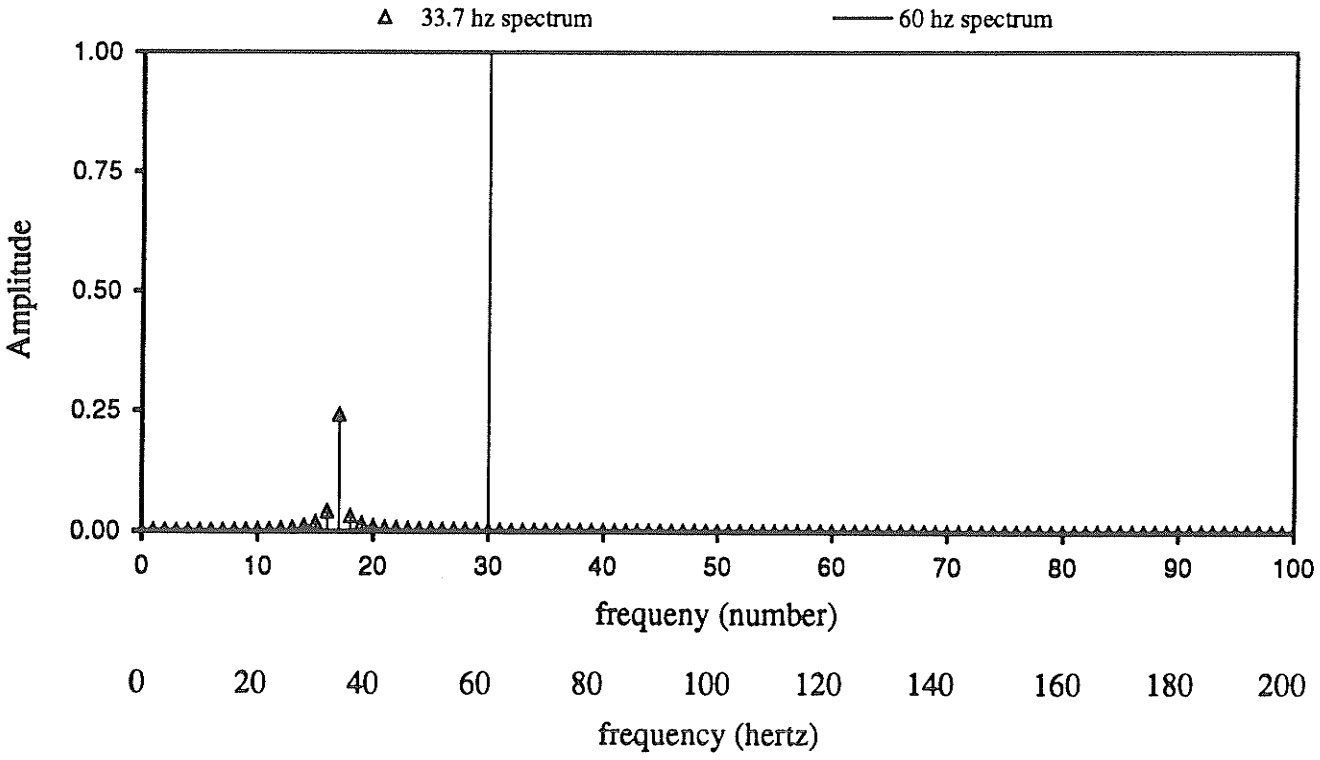

Figure 4.4: The Discrete Fourier Transform over a Time Interval of 0.5 Seconds

As can be seen, the 60 hz waveform shows up very clearly on the spectrum with exactly the correct amplitude, while the 33.7 hz signal can by no means be accurately measured or even identified. It is therefore quite apparent that this limited spectrum is of little use as it stands, and a much denser spectrum is required.

In order to obtain a denser spectrum (i.e. one with the bands much closer together) the interval of analysis in the time domain must be greatly increased. Figure 4 .4 on the previous page shows a discrete transform of the curve in Figure 4 .2 where a time interval of 0.5 seconds is now used. (This interval once again contains an integer number of cycles of the 60 hz waveform.) Although the amplitude and the precise frequency of the 33.7 hz signal are still not exactly known, a very good approximation to these values can now be made.

Ideally, the time interval should be chosen in such a manner that it contains an integer number of periods of all frequencies present, but in practice this becomes very difficult when an entire host of sub– and supersynchronous frequencies exist. Therefore, for the purpose of this thesis, a 4 second time interval will be used, in order to yield a fairly dense discrete transform with an incremental frequency of $\Delta f = 0.25 \ hz$. Very minor modifications to this time interval may be required to ensure that a minimum amount of noise is introduced by the fundamental which may drift slightly from its 60 hz value.

Of course, the problems discussed in this section only manifest themselve when the Discrete Fourier Transform is used. In practice, use of a continuous spectrum would eliminate these problems. Perhaps an even more useful tool to use in a practical setting, however, would be a phase locked loop. Although their primary use in power systems is to determine the zero crossing of the fundamental, they can be modified to yield

amplitude and phase information of known non-fundamental frequencies in a voltage or current waveform.

4 .3 The Electro-Mechanical System to be Simulated

The multimass machine model to be simulated consists of two turbines and one generator, and the mechanical specifications for this system were given in Section 2.7. In Chapter 2 it was also stated that the excitation system need generally not be modelled, therefore a constant field voltage is used in the simulation. Finally, since the machine is operating in the steady state and any disturbances are very minor, the governor system is not required and a constant driving torque matched to the load and field voltage can be employed.

The system to be simulated is therefore very simple as shown in Figure 4 .5 .

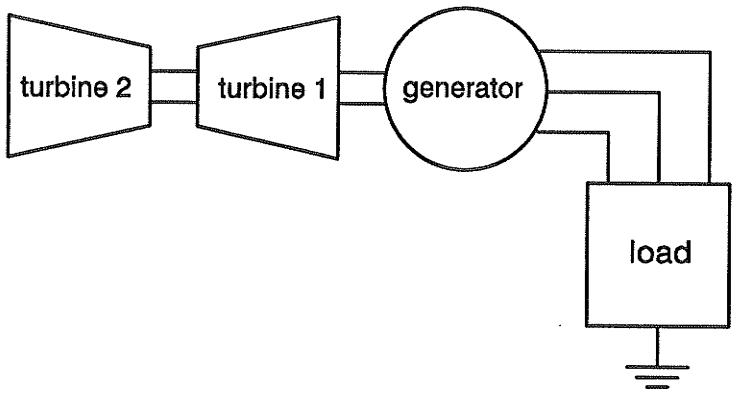

Figure 4 .5 : The System to be Simulated.

Since the above system is running stably in the steady state, a small amount of positive damping must exist. This positive damping will

eventually eliminate the presence of all resonant oscillations. (Otherwise the system would be unstable.) Therefore in order to study these resonant oscillations, a small disturbance must be introduced to initiate them.

The disturbance to be used will be a small impulse superimposed on the constant input torque supplied to the turbines. An impulse is chosen because it is guaranteed to excite all resonances without introducing other changes to the "steady state" system.

4 .4 Simulation of the No Load Synchronous Machine

Simulation of the system in Figure 4 .5 under "no load" is actually carried out using an extremely large resistive load (R = 100 pu.).

This is required because no mechanical damping is included in the model (as explained in Section 2.7) and if the machine were run open circuited, it would not be possible to achieve stable operation.

As discussed in Section 4.2, at least four seconds of simulation are required (after the disturbance which initiates the resonant oscillations) in order to obtain a discrete Fourier spectrum with the desired resolution of 0.25 hertz.

Figure 4 .6 shows the normalized Fourier spectrum of the phase A generator terminal voltage at a time directly following the application of a small disturbance.

As can be seen the disturbance has very slightly affected the base shaft speed of the machine. Although this effect is not desired and would not occur if the machine were operating in a normal system it has basically no impact (good or bad) on any calculations regarding resonant oscillations.

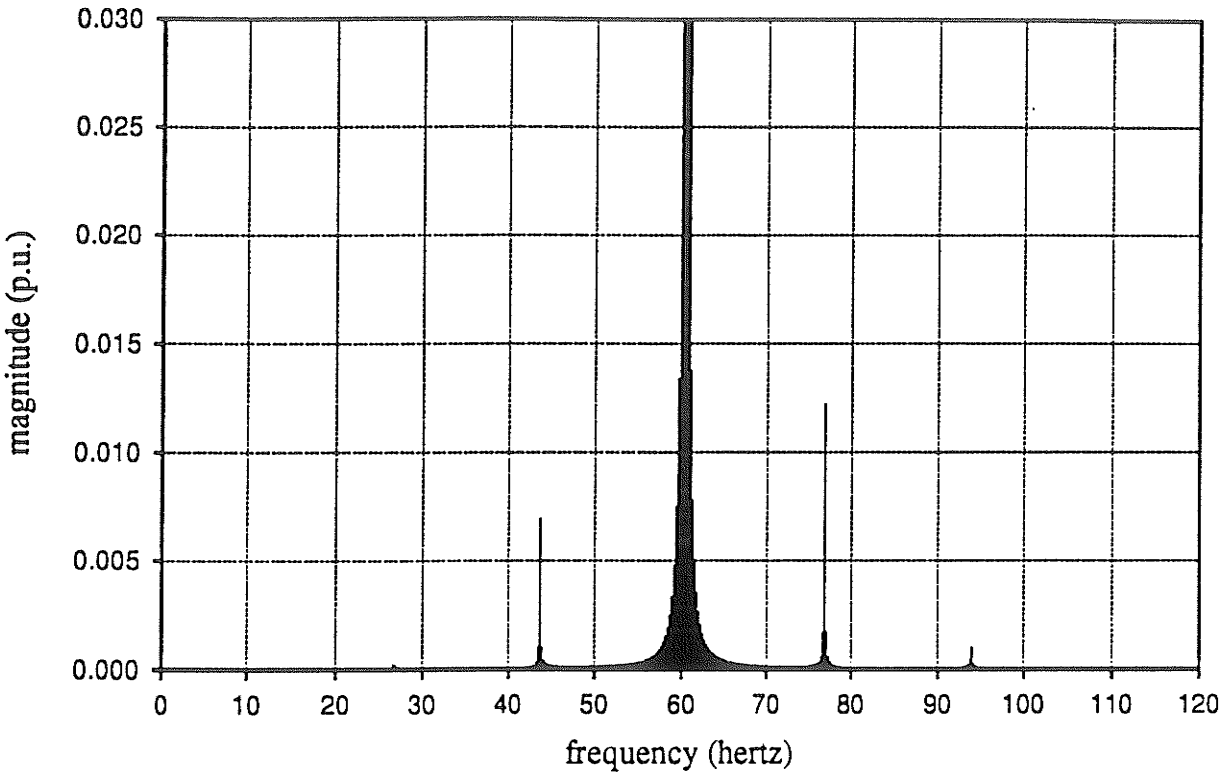

Figure 4 .6 : The Fourier Spectrum of the Generator Terminal Voltage – The No Load Case.

From Figure 4 .6 the resonant frequencies can quickly be determined and compared with the values expected by the eigenvalue analysis of Chapter 2. These are compared in Table 4 .1 . For all practical purposes the theoretical and simulated resonant frequencies can be considered identical.

Table 4 .1 : Comparison of the Theoretical and Simulated Resonant Frequencies.

Mode Number	Resonant Frequency from Theory	Resonant Frequency from Simulation
Mode 1	16.61	16.60
Mode 2	33.61	33.65

Next, the side band amplitudes of Figure 4 .6 can be employed to calculate the amplitudes of the resonant oscillations at f_{n1} and f_{n2}.

Theoretically, either the upper or lower set of side bands can be used to find the oscillation amplitudes, but in practice, the upper bands should be used because they are larger. Not only can the larger bands be measured with more accuracy, but more importantly, they are much less susceptible to accuracy losses caused by background noise.

Since the magnitudes of the bands at $f_0 + f_{n1}$ and $f_0 + f_{n2}$ are 0.01223 and 0.001291 respectively, the generator shaft oscillation amplitudes are found to be

$$\frac{\beta_1(\omega_o + \omega_{n1})}{2\omega_o} = 0.01223 \qquad \beta_1 = 0.01916$$

$$\frac{\beta_2(\omega_o + \omega_{n2})}{2\omega_o} = 0.001004 \qquad \beta_2 = 0.001291 \ .$$

(4 .2)

Therefore from equations 3 .38 and 3 .39 the generator shaft position and speed are given below (there could be a phse shift for each oscillation, but it cannot be determined by the analysis presented.)

$$\theta_{gen} = \omega_o t + 0.01916 \sin 2\pi f_{n1} t + 0.001291 \sin 2\pi f_{n2} t$$

(4 .3)

$$\omega_{gen} = \omega_o + 1.995 \cos 2\pi f_{n1} t + 0.2729 \cos 2\pi f_{n2} t$$

(4 .4)

Employing the mode shapes calculated for this particular turbine–generator yields the speed and position of each of the turbines.

$$\theta_{turb1} = \omega_o t + 0.01313 \sin 2\pi f_{n1} t + 0.001746 \sin 2\pi f_{n2} t$$

(4 .5)

$$\omega_{turb1} = \omega_o t + 1.367 \cos 2\pi f_{n1} t + 0.3691 \cos 2\pi f_{n2} t$$

(4 .6)

$$\theta_{turb2} = \omega_o t + 0.001717 \sin 2\pi f_{n1} t + 0.004463 \sin 2\pi f_{n2} t$$

(4 .7)

$$\omega_{turb2} = \omega_o + 0.1788 \cos 2\pi f_{n1} t + 0.9437 \cos 2\pi f_{n2} t$$

(4 .8)

Unfortunately, the instantaneous position and speed of each mass are not normally available on EMTDC [17]. However, minor modifications to the code allow output of at least the individual mass speeds. This is sufficient to test the accuracy of the theory because mass speed and position are not independant quantities.

Figure 4 .7 shows the simulated shaft speeds of each of the three masses after the application of a disturbance at 0.1 seconds. The Fourier spectra of the generator speed and the two turbine speeds are given in Figure 4 .8 . These spectra show the actual oscillating amplitudes of each mass at each of the two resonant frequencies. They also include the theoretically predicted oscillating amplitudes and frequencies for the sake of comparison.

The simulated and theoretically predicted results are compared in tabular form as well. This is shown in Table 4 .2 below, where the percentage errors between theory and simulation are shown in Table 4 .3 .

Table 4 .2 : Comparison of the Theoretical and Simulated Oscillation Amplitudes – No Load.

mass	Oscillating Amplitude at 16.6 hz		Oscillating Amplitude at 33.6 hz	
	predicted	measured	predicted	measured
generator	1.995	1.997	0.2729	0.2749
turbine 1	1.367	1.373	0.3691	0.3709
turbine 2	0.1788	0.1863	0.9437	0.9510

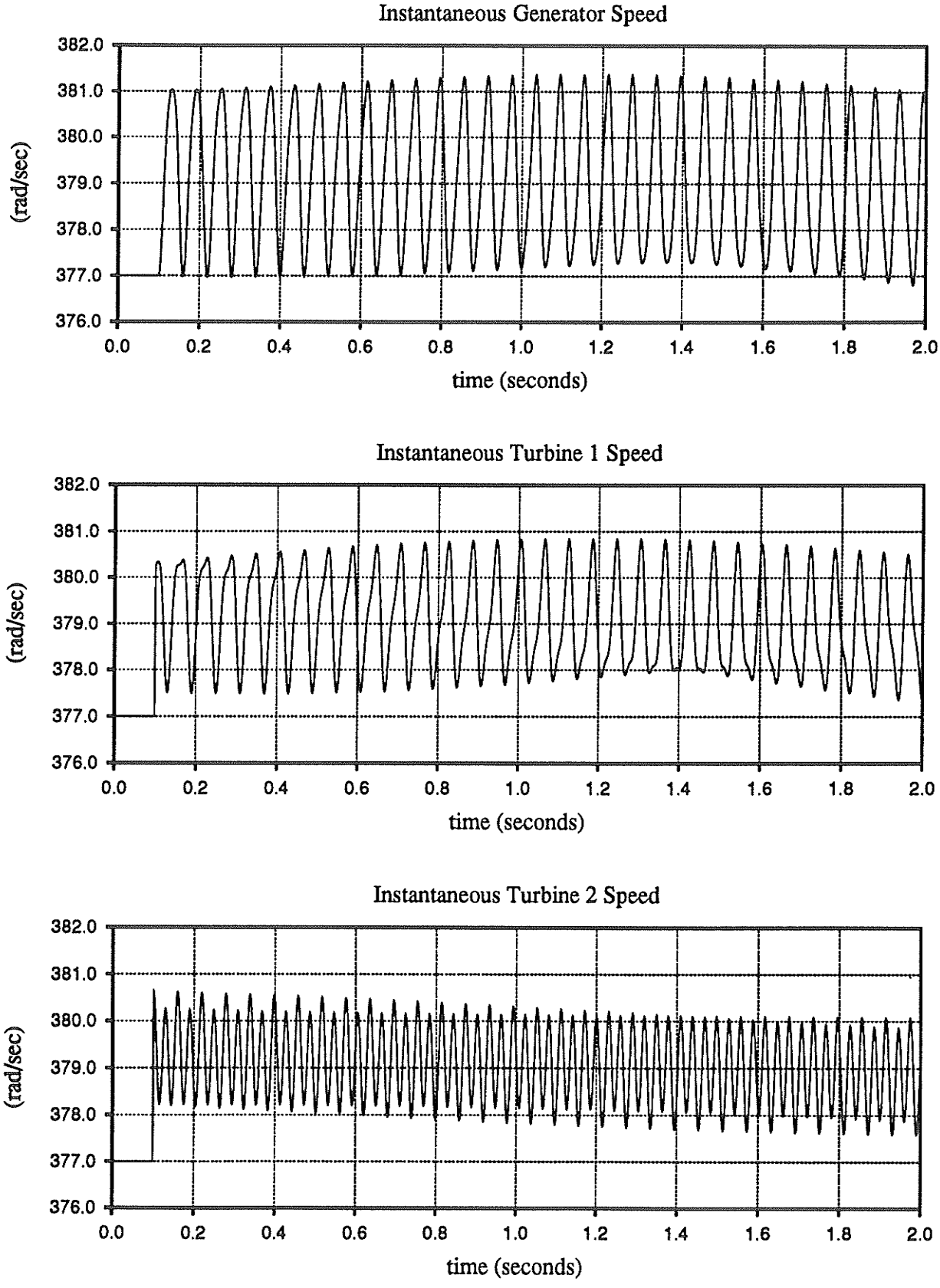

Figure 4.7: The Instantaneous Speed of each Mass

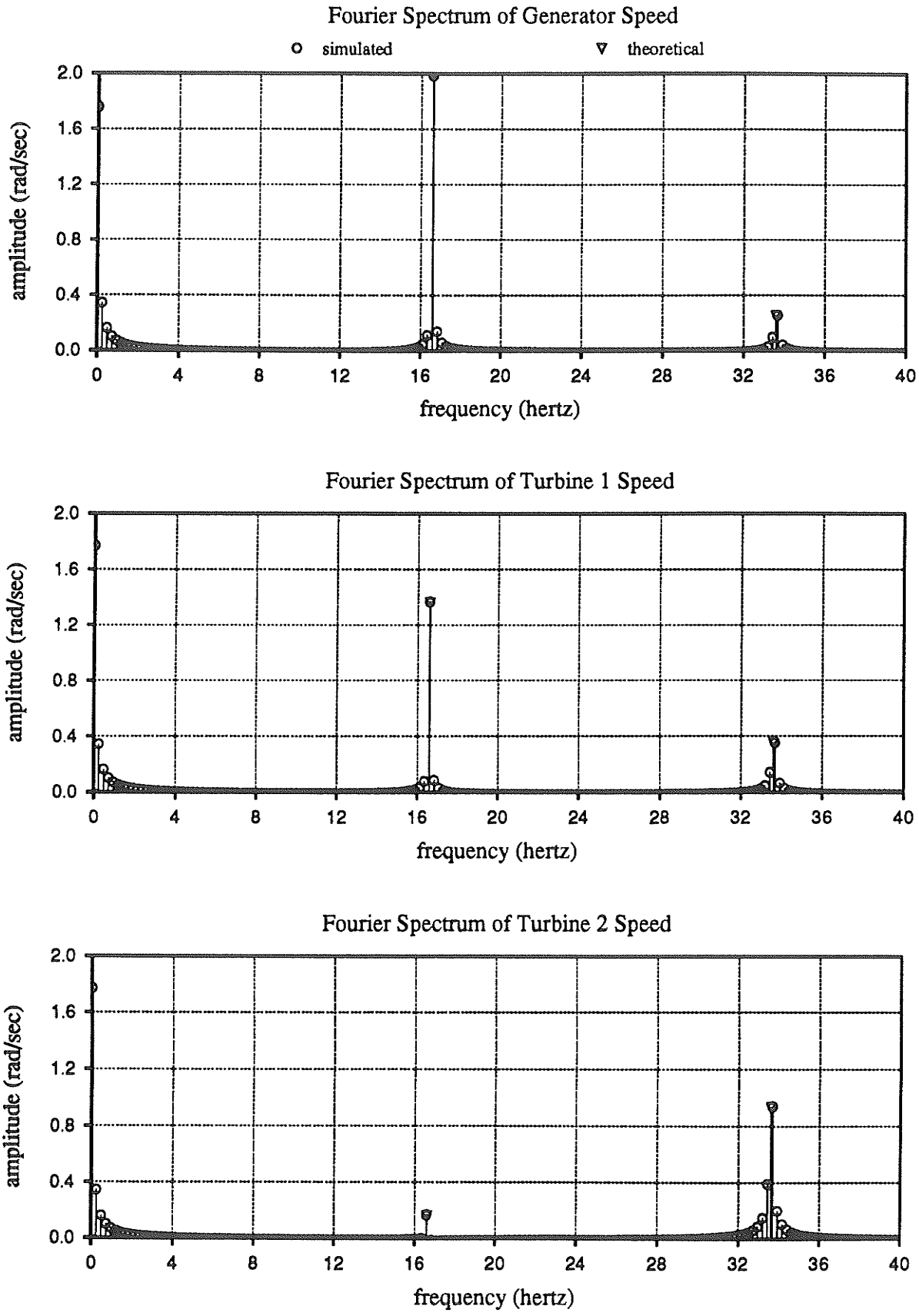

Figure 4.8: The Actual and Theoretical Fourier Spectra of the Mass Speeds

Table 4 .3 : The Percentage Error in the Theoretical Oscillation Amplitudes – No Load.

mass	Percent Error in the Theoretical Amplitude at 16.6 hz	Percent Error in the Theoretical Amplitude at 33.6 hz
generator	– 0.1 %	– 0.7 %
turbine 1	– 0.4 %	– 0.5 %
turbine 2	– 4.0 %	– 0.8 %

As is evident, the predicted amplitudes at 33.7 hz fall about 4% shy of the simulation results. The reason for this becomes apparent when looking back at the voltage spectrum given in Figure 4 .6 . It can be seen there that the band at (approximately) 94 hz is quite small and it is not surprising that the background noise introduces a certain degree of error.

The accuracy of the modal theory presented in Chapter 2 can also be checked with simulation results, to insure that all approximations performed are reasonable. The theoretical mode shapes, repeated from Chapter 2 are given in Table 4 .4 .

Table 4 .4 : The Theoretical Mode Shapes of the Turbine – Generator.

mass	Mode 1 f_1 = 0 hz	Mode 2 f_2 = 16.6 hz	Mode 3 f_3 = 33.6 hz
generator	1	1	1
turbine 1	1	– 0.6852	1.353
turbine 2	1	– 0.0896	–3.458

Using the simulation results given in Figure 4 .8 the magnitudes of the true mode shapes of the turbine generator can be determined. These are shown in Table 4 .5 .

Table 4 .5 : The Mode Shapes of the Turbine – Generator from Simulation

mass	Mode 1 $f_1 = 0$ hz	Mode 2 $f_2 = 16.6$ hz	Mode 3 $f_3 = 33.6$ hz
generator	1	1	1
turbine 1	1	0.6877	1.349
turbine 2	1	0.0933	3.459

Comparison of the above two tables shows that the simulated and theoretical mode shape are indeed almost the same. The percent error in the theoretical mode shapes is shown below.

Table 4 .6 : The Percent Error in the Theoretical Mode Shapes.

mass	Error in the Theoretical Amplitude at 16.6 hz	Error in the Theoretical Amplitude at 33.6 hz
generator	0 % by definition	0 % by definition
turbine 1	– 0.4 %	0.3 %
turbine 2	– 4.0 %	0.0 %

The theory clearly produces quite accurate results for the no load turbine–generator. The next logical step is therefore to see if the theory holds equally well when the machine is subject to arbitrary load conditions.

4 .5 The Machine Under Load

Several load conditions will be considered in this section. All the cases that will be presented, however, will be with the turbine–generator run at or near its rated MVA. This approach is taken because it represents a

worst case scenario and it corresponds to the maximum discrepancies between theoretical and simulated results. Although this statement may not seem self-evident, its validity was indeed checked through many comparison tests.

Three load cases will be investigated. The first simply comprises a purely resistive load with R = 1.0 p.u. The second is chosen to be an RL load (Z = 1.0 p.u.) with a power factor of 0.707 . The final case will consist of an active, HVDC load. In this case the validity of the theory has not expressly been proven; however since the theory is valid for a completely arbitrary passive load, it should prove to be of some use in analyzing the behaviour of turbine-generators connected to HVDC link as well.

4 .5 .1 The Resistive Load

The system to be modelled here is again shown in Figure 4 .5 ,where the load is now purely resistive with a magnitude of 1.0 pu.

Once again the phase A terminal voltage of the generator is analyzed and its normalized Fourier spectrum is shown in Figure 4 .9 . From this spectrum and the modal theory the speeds of the three masses are calculated (again, the possiblity of a phase shifts are ignored).

$$\omega_{gen} = \omega_o + 1.564 \cos 2\pi f_{n1} + 0.2749 \cos 2\pi f_{n2} t \qquad (4.9)$$

$$\omega_{turb1} = \omega_o + 1.072 \cos 2\pi f_{n1} t + 0.3718 \cos 2\pi f_{n2} t \qquad (4.10)$$

$$\omega_{turb2} = \omega_o + 0.1402 \cos 2\pi f_{n1} t + 0.9507 \cos 2\pi f_{n2} t \qquad (4.11)$$

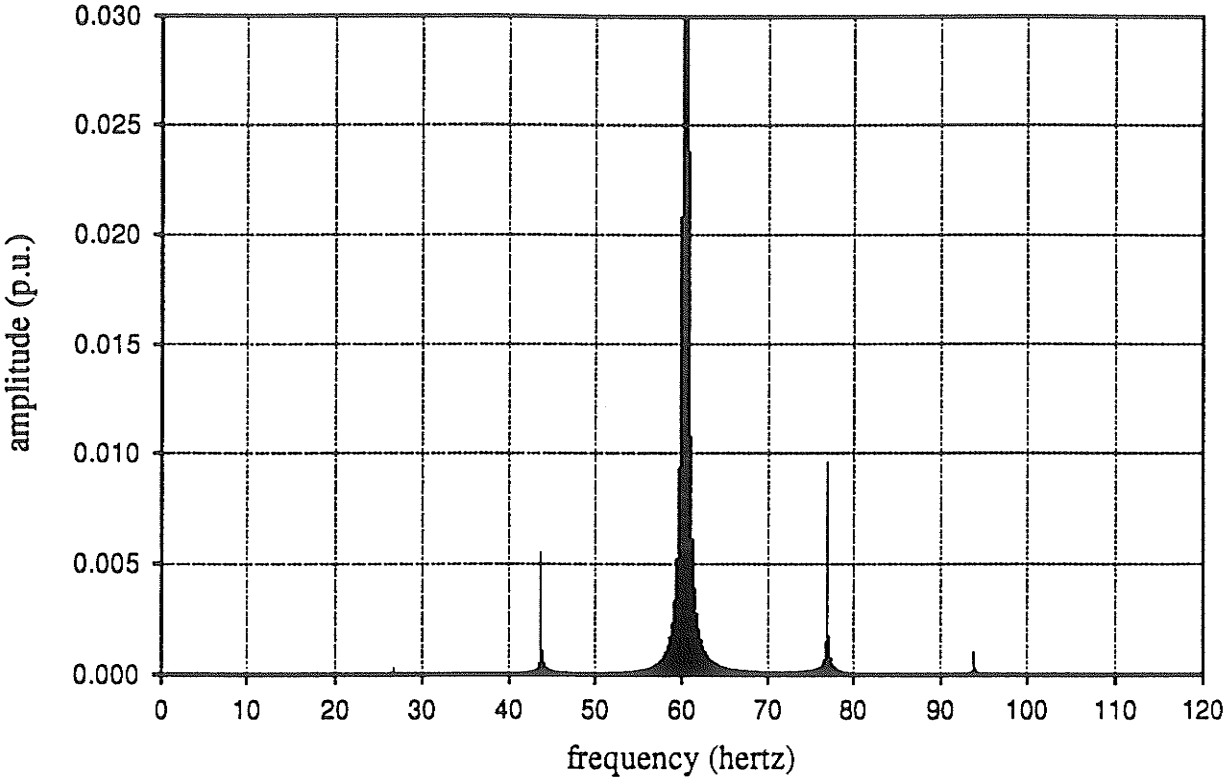

Figure 4 .9 : The Fourier Spectrum of the Generator Terminal Voltage – The Resistive Load Case.

Figure 4 .10 gives the actual spectra of the mass speeds. The predicted oscillating amplitudes found from the theory are also shown on these plots. The exact oscillating amplitudes are given in Table 4 .7 and the percent errors between the theoretical and simulated results are given in Table 4 .8 .

Table 4 .7 : Comparison of the Theoretical and Simulated Oscillating Amplitudes – Resistive Load of 1.0 pu.

mass	Oscillating Amplitude at 16.6 hz		Oscillating Amplitude at 33.6 hz	
	predicted	measured	predicted	measured
generator	1.564	1.619	0.2749	0.2793
turbine 1	1.072	1.115	0.3718	0.3716
turbine 2	0.1402	0.1519	0.9507	0.9633

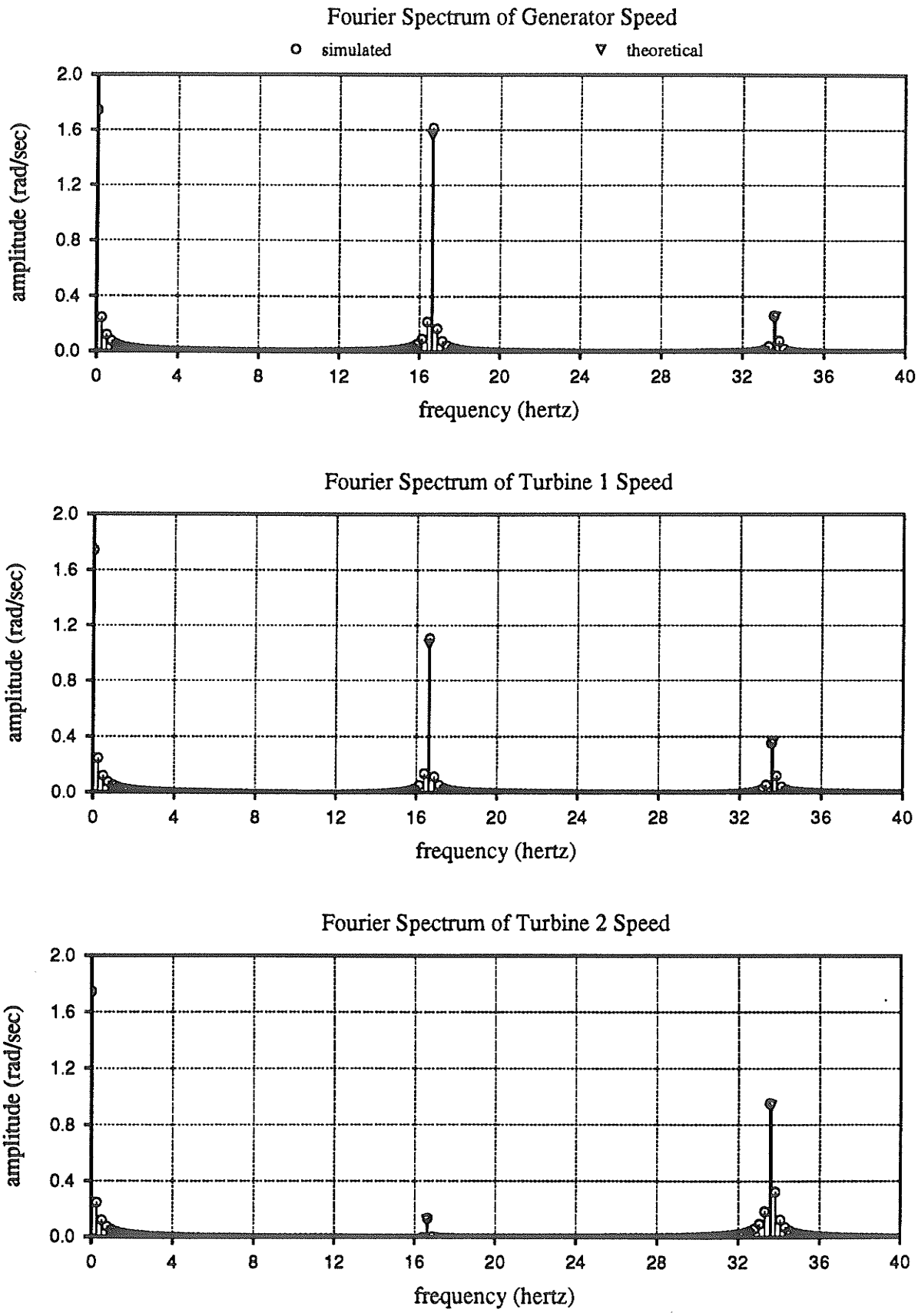

Figure 4.10: The Theoretical and Simulated Fourier Spectra of the Mass Speeds

Table 4 .8 : The Percent Error in the Theoretical Oscillation Amplitudes – Resistive Load of 1.0 p.u.

mass	Error in the Theoretical Amplitude at 16.6 hz	Error in the Theoretical Amplitude at 33.6 hz
generator	– 3.4 %	– 1.6 %
turbine 1	– 3.9 %	+ 0.1 %
turbine 2	– 7.7 %	– 1.3 %

Although the predicted oscillation amplitudes are not quite as accurate as in the no load case of the previous section, the errors are still quite acceptable. This increased error is partially due to the neglect of the armature resistance which now plays a role, and also the damping introduced by the resistive load which causes some distortion of the Fourier spectrum. (Once again the error is largest in the 33.6 hz oscillation due to the small size of its corresponding band, at 94 hz, on the Fourier Spectrum.)

4 .5 .2 The RL Load

In order to demonstrate that the theory holds for an arbitrary RL load many simulations should be run and all results should be checked against thee theory. Such a rigorous verification of the theory was indeed performed, however, for the sake of brevity only one sample RL load will be considered. Also, introduction of a capacitor into the circuit has no substantial impact on the accuracy of the theory; however this can only be proven by simulation if stable operation exists.

Figure 4 .11 shows the normalized Fourier Spectrum of the phase A terminal voltage. From this spectrum the mass speeds are calculated to be as shown on the following page (phase information ignored).

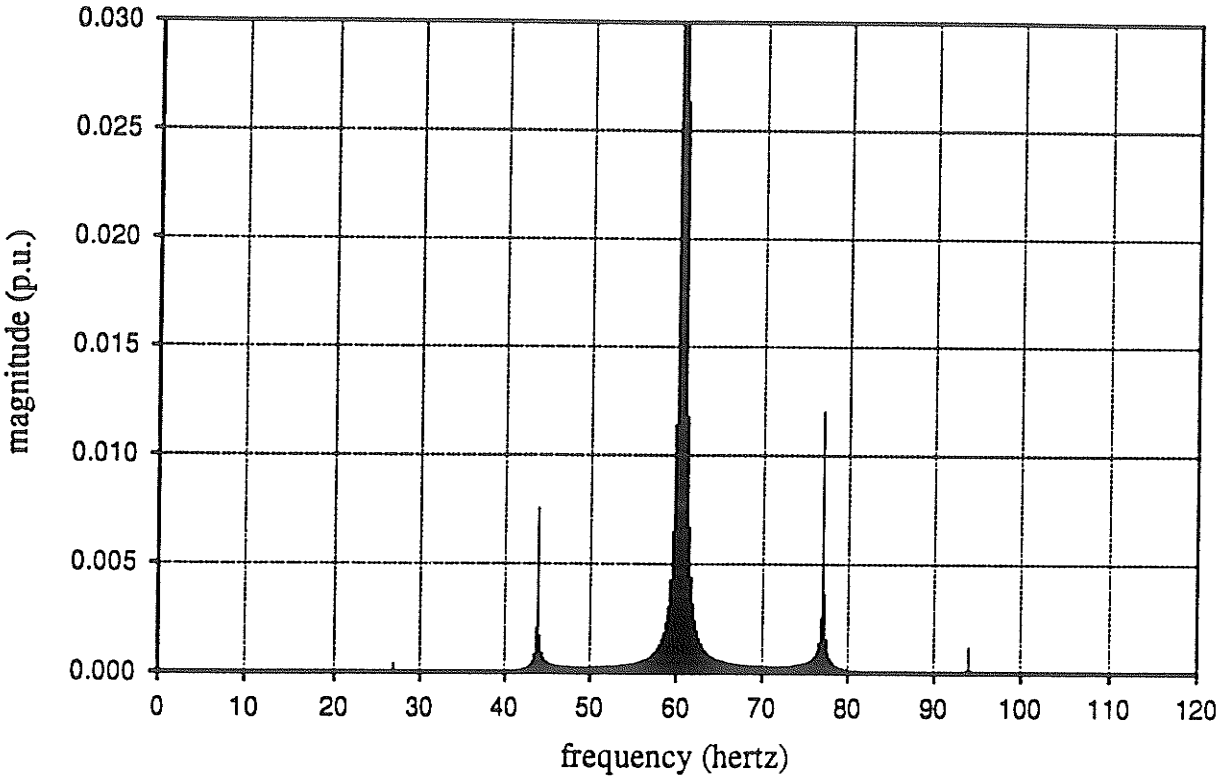

Figure 4 .11 : The Fourier Spectrum of the Generator Terminal Voltage – The RL Load Case.

$$\omega_{gen} = \omega_o + 1.960 \cos 2\pi f_1 t + 0.3165 \cos 2\pi f_2 t \qquad (4.12)$$

$$\omega_{turb1} = \omega_o + 1.343 \cos 2\pi f_1 t + 0.4282 \cos 2\pi f_2 t \qquad (4.13)$$

$$\omega_{turb2} = \omega_o + 0.1756 \cos 2\pi f_1 t + 1.095 \cos 2\pi f_2 t \qquad (4.14)$$

Figure 4 .12 graphically compares the theoretical and simulated mass. The exact oscillating amplitudes are given in Table 4 .9 and the percent errors between the theoretical and simulated results are given in Table 4 .10 .

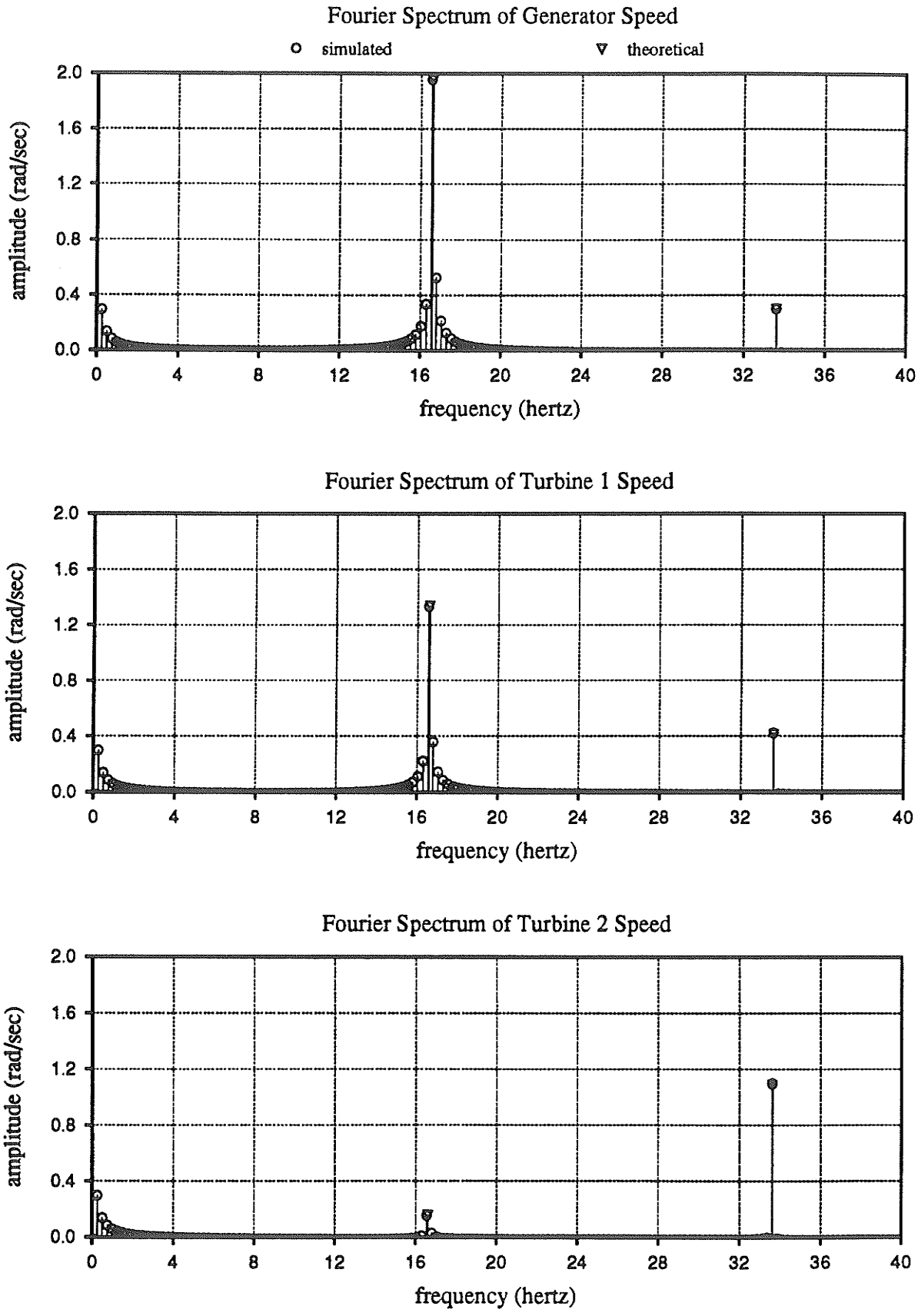

Figure 4.12: The Theoretical and Simulated Fourier Spectra of the Mass Speeds

Table 4 .9 : Comparison of the Theoretical and Simulated Oscillation Amplitudes – RL Load of 1.0 pu, 0.707 pf.

mass	Oscillating Amplitude at 16.6 hz		Oscillating Amplitude at 33.6 hz	
	predicted	measured	predicted	measured
generator	1.960	1.958	0.3165	0.3212
turbine 1	1.343	1.340	0.4282	0.4371
turbine 2	0.1756	0.1747	1.095	1.107

Table 4 .10 : The Percentage Error in the Theoretical Oscillation Amplitudes – RL Load of 1.0 pu, 0.707 pf.

mass	Error in the Theoretical Amplitude at 16.6 hz	Error in the Theoretical Amplitude at 33.6 hz
generator	0.1 %	– 1.5 %
turbine 1	0.2 %	– 2.0 %
turbine 2	0.5 %	– 1.1 %

Three loads with very different characteristics have now been analyzed: a no load case, a full load resistive case and a highly inductive full load case. Tables 4 .3 , 4 .8 and 4 .10 show the percent error between the theory and simulation results for the three cases. Comparing these three tables now shows that the load conditions really only have a marginal influence on the accuracy of the theoretical calculations. By extension, it should be clear that the inclusion of documentation on other load scenarios will introduce no new insights into the area.

4 .5 .3 The HVDC Load

The theory has now been validated for a variety of passive load conditions. It is conjecture that the same analysis technique can be usefully applied to other types of loads. A test of this conjecture will be performed which consists of connecting the multimass machine model to an HVDC load network. The HVDC network to be used will be a modification of the CIGRE Benchmark model [18]. All power at the rectifier end will be supplied, through a transformer, by the 588 MVA machine which has already been analyzed. The power demands of the system are modified so that the machine is operating near its full load rating and the compensation on either side of the link is adjusted accordingly.

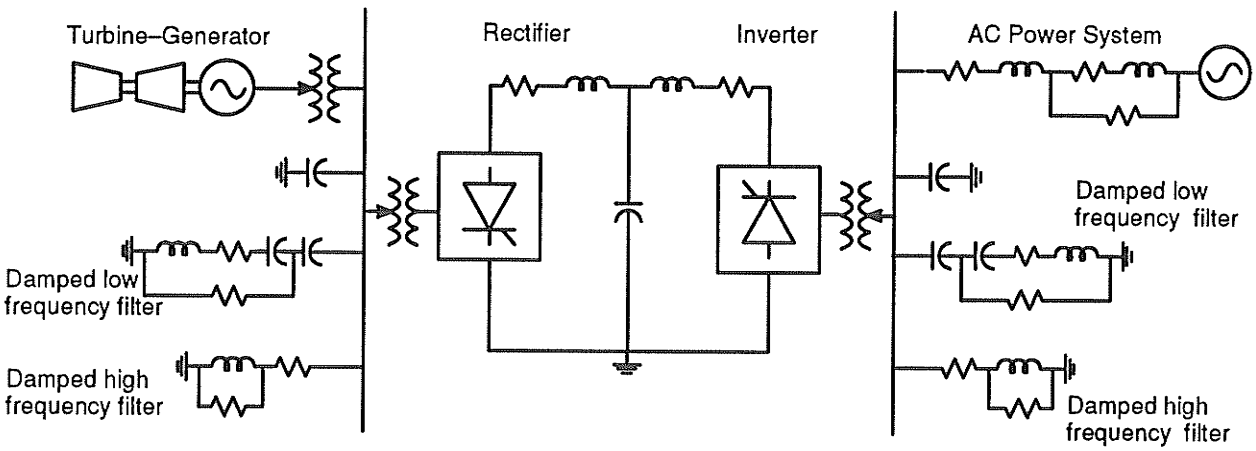

Figure 4 .13 : The Multimass Turbine-Generator connected to the CIGRE Benchmark Model

Although a completely static field voltage is still employed on the machine, all DC link controls are left unmodified and fully enabled. The basic system configuration is as shown in Figure 4 .13 .

Just as in the previous cases, the phase A generator voltage is analyzed and its normalized Fourier spectrum is shown in Figure 4 .14 below. Due to the large size of the new network, simulation was only carried out for 2 seconds after the application of the disturbance. For this reason the spectrum of Figure 4 .14 has a frequency increment of $\Delta f = 0.5$ hz rather than 0.25 hz as in the previous cases.

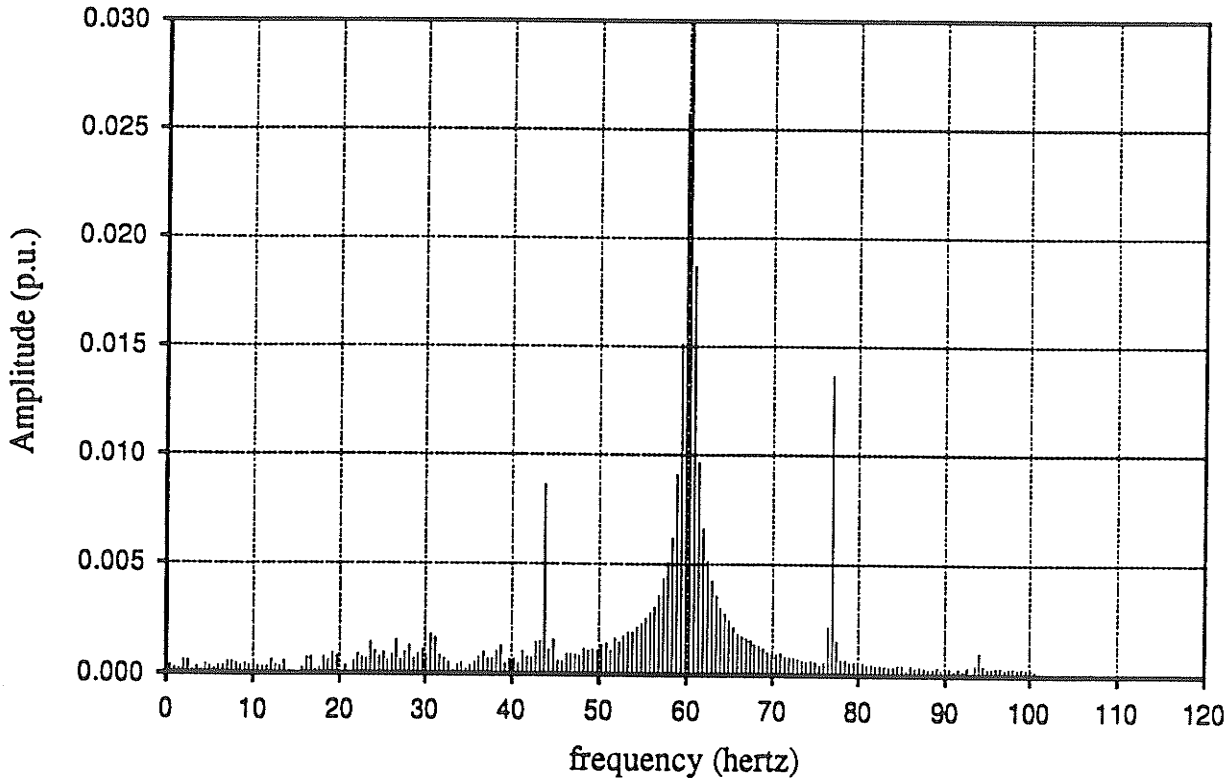

Figure 4 .14 : The Fourier Spectrum of the Generator Terminal Voltage – The HVDC Load Case

Unlike the spectra of the previous sections, a substantial amount of noise is now present in the subsynchronous domain. This is a consequence of the normally operating HVDC controls which are reacting to the system disturbance that initiated the turbine–generator shaft oscillations [19]. This noise has the effect of masking the lower subsynchronous bands and therefore, only the upper bands of the spectrum can be used to determine the amplitudes of the shaft oscillations.

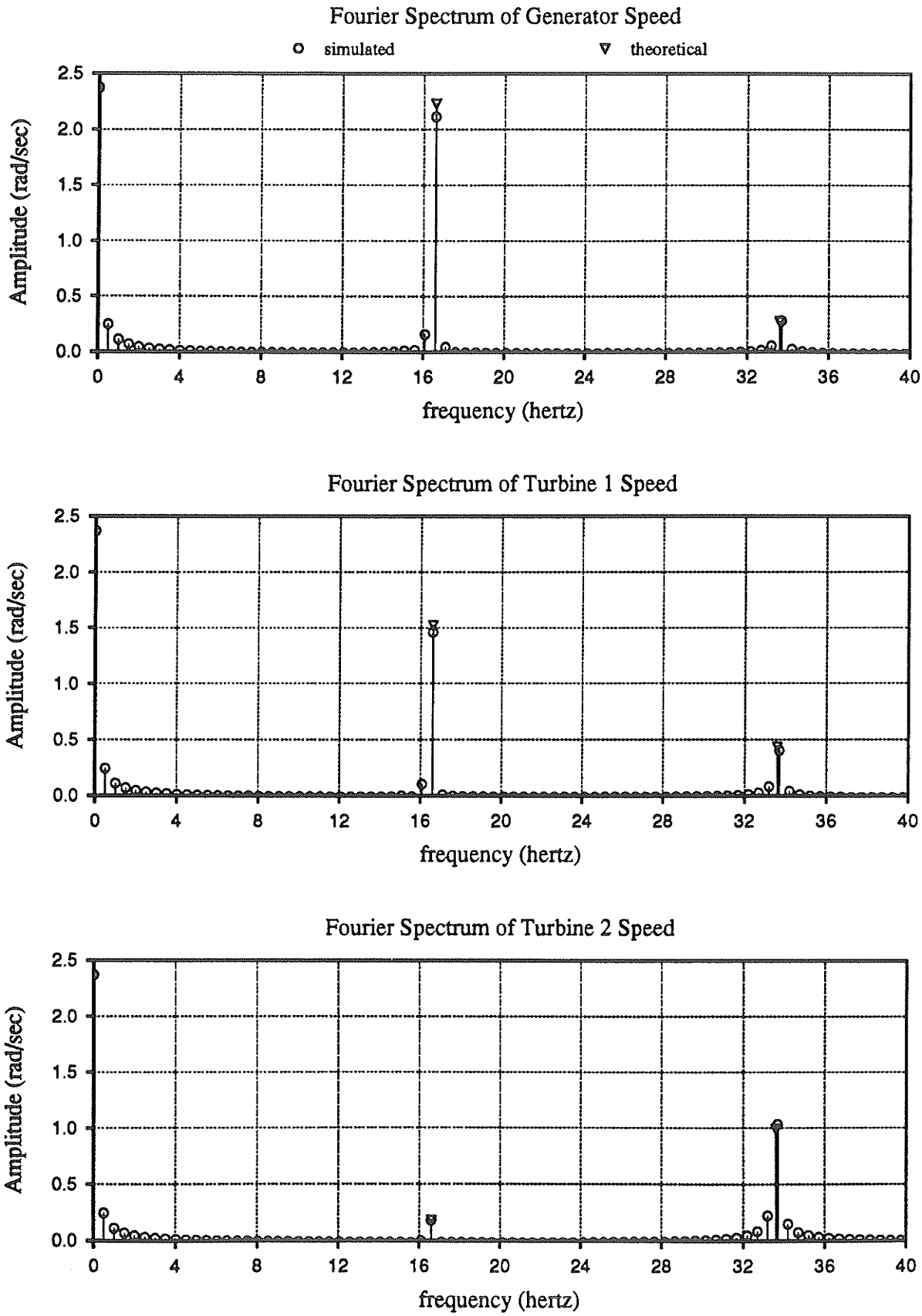

Figure 4.15: The Theoretical and Simulated Fourier Spectra of the Mass Speeds

Figure 4 .15 graphically shows the simulated and theoretical turbine–generator shaft oscillation amplitudes for the HVDC load case. The exact amplitudes are also shown in Table 4 .11 , while the percent error in the theoretical values is given in Table 4 .12 .

Table 4 .11 : Comparison of the Theoretical and Simulated Oscillation Amplitudes – The HVDC Load.

mass	Oscillating Amplitude at 16.6 hz		Oscillating Amplitude at 33.6 hz	
	predicted	measured	predicted	measured
generator	2.232	2.115	0.2901	0.2973
turbine 1	1.529	1.468	0.4505	0.4204
turbine 2	0.2000	0.1986	1.003	1.044

Table 4 .12 : The Percentage Error in the Theoretical Oscillation Amplitudes – The HVDC Load.

mass	Error in the Theoretical Amplitude at 16.6 hz	Error in the Theoretical Amplitude at 33.6 hz
generator	5.5 %	– 2.4 %
turbine 1	4.2 %	7.2 %
turbine 2	0.7 %	– 3.9 %

As can be seen from the spectra of Figure 4 .15 , and the percent errors of Table 4 .12 , the conjecture does, in fact, prove to hold for the

HVDC load case. Although the theory produces somewhat less accurate results than when a passive load is used, the errors which exist here are by no means excessive.

This load case is significant because it demonstrates the validity of the theory even when a turbine–generator is connected into a system which contains active elements, run by complex control structures.

Chapter 5

Conclusions and Recommendations

5 .1 Conclusions

A process based on the Fourier Transform of a machine's terminal voltage was proposed, to measure the frequency and amplitude of subsynchronous resonances in a multimass turbine–generator system. A theoretical mode shape model was developed for a three mass system to relate generator terminal measurements to the amplitude of shaft angle oscillations. Although only a 3 mass model was investigated, extension of the theory to 4 or more masses requires only a straightforward recalculation of the mode shapes.

The theory was first developed for an unloaded generator and then expanded to include arbitrary load conditions. Rigorous testing of the theory was performed using EMTDC simulation, and the results for selected passive load configurations were presented. The applicability of the theory to an active HVDC load was also demonstrated. The accuracy of all theoretical results proved to be very acceptable.

The information obtained by this analysis technique has, of course, many applications in the areas of system control and shaft stress

monitoring. This process should prove to be an economical and practical alternative to the installation of shaft angle sensors which are used in many applications today.

5 .2 Recommendations

There is a great deal of room for further work in the area of subsynchronous oscillation measurement. The analysis presented in this thesis has related shaft oscillation amplitudes to the Fourier spectrum of the terminal voltage waveform. When implementing such a process, it would, however, be beneficial to perform the spectral analysis on the machine's internal voltage rather than the terminal voltage. This would have the effect of increasing the accuracy of the calculated oscillation amplitudes.

Perhaps the most meaningful extension of this work would be to replace the Fourier spectral analysis with phase locked loop technology. Since the oscillating frequencies of the turbine–generator are known in advance, phase locked loops could be tuned to lock on to and measure the amplitude of the side bands in the voltage spectrum. Not only would this be an extremely practical extension, but it would also yield phase information about the subsynchronous oscillations. This information could be directly employed in the control networks of HVDC links.

REFERENCES

[1] IEEE SSR Working Group, *"Proposed Terms and Definitions for Subsynchronous Oscillations,"* IEEE Transactions PAS–99, No. 2, 1980, pp. 506–511.

[2] H. Rustebakke and C. Concordia, *"Self–Excited Oscillations in a Transmission System Using Series Capacitors,"* IEEE Transactions PAS–89, No. 7, 1970, pp. 1504–1512.

[3] C. Concordia and G.K. Carter, *"Negative Damping of Electrical Machinery,"* AIEE Transactions, Vol. 60, March, 1941, pp. 116–119.

[4] J.W. Butler and C. Concordia, *"Analysis of Series Capacitor Application Problems,"* AIEE Transactions, Vol. 56, 1937, pp. 975–978.

[5] J.W. Ballance and S. Goldberg, *"Subsynchronous Resonance in Series Compensated Transmission Lines,"* IEEE PES Winter Meeting, New York, N.Y., 1973, pp. 1649–1658.

[6] M. Bahrman, E.V. Larsen, R.J. Piwko, and H.S. Patel, *"Experience with HVDC Turbine–Generator Torsional Interaction at Square Butte,"* IEEE Transaction PAS–99, No. 3, 1980, pp. 966–975.

[7] R.J. Piwko, M.D. Kankam, C.T. Wu, and K.J. Peterson, *"Dealing with Torsional Interaction Between HVDC Convertors and Turbine Generators,"* American Power Conference Proceedings, 1988, pp. 401–407.

[8] Y.Y. Hsu and L. Wang, *"Modal Control of and HVDC System for the Damping of Subsynchronous Oscillations,"* IEEE Proceedings, Vol. 136, No. 2, 1989, pp. 78–86.

[9] B. Adkins and R.G. Harley, *"The General Theory of Alternating Current Machines,"* John Wiley & Sons, Inc., New York, 1975.

[10] O.I. Elgerd, "*Electric Energy Systems Theory: An Introduction,*" McGraw–Hill, Inc., Toronto, 1971.

[11] P.M. Anderson and A.A. Fouad, "*Power System Control and Stability,*" The Iowa State University Press, Ames, Iowa, 1977.

[12] P.M. Anderson, B.L. Agrawal, and J.E. Van Ness, "*Subsynchronous Resonance in Power Systems,*" IEEE Press, Inc., New York, 1990.

[13] R.C. Dorf, "*Modern Control Systems,*" 4 th. edition, Addison–Wesley Publishing Company, Don Mills, Ontario, 1986.

[14] J.J. D'Azzo, et al., "*Linear Control System Analysis & Design,*" McGraw–Hill Book Company, Toronto, 1988.

[15] W. Kaplan, "*Advanced Mathematics for Engineers,*" Addison–Wesley Publishing Company, Don Mills, Ontario, 1981.

[16] E.O. Brigham, "*The Fast Fourier Transform and its Application,*" Prentice Hall, Inc., Englewood Cliffs, New Jersey, 1988.

[17] "*EMTDC User's Manual*", Version 3, Manitoba HVDC Research Centre, Winnipeg, Canada, 1988.

[18] "CIGRE Benchmark Model for DC Controls", Electra, Vol. 135, April 1991, pp 54 – 73.

[19] K.R. Padiyar, "*HVDC Power Transmission Systems,*" John Wiley & Sons, Toronto, 1990.

Appendix A

Mathcad 3.0 File

Calculation of Mode Shapes

GENERATOR TURBINE 1 TURBINE 2

$j1 := 10500$ $j2 := 8590$ $j3 := 14200$ $k12 := 105000000$

$k23 := 178000000$

$$N := \begin{bmatrix} \sqrt{j1} & 0 & 0 \\ 0 & \sqrt{j2} & 0 \\ 0 & 0 & \sqrt{j3} \end{bmatrix} \qquad K := \begin{bmatrix} k12 & -k12 & 0 \\ -k12 & k12+k23 & -k23 \\ 0 & -k23 & k23 \end{bmatrix}$$

$$B := N^{-1} \cdot K \cdot N^{-1}$$

$$\lambda := \text{eigenvals}(B)$$

$$\lambda = \begin{bmatrix} 1.089604 \cdot 10^4 \\ 0 \\ 4.458445 \cdot 10^4 \end{bmatrix} \qquad D := \begin{bmatrix} \lambda_1 & 0 & 0 \\ 0 & \lambda_0 & 0 \\ 0 & 0 & \lambda_2 \end{bmatrix} \qquad D = \begin{bmatrix} 0 & 0 & 0 \\ 0 & 1.09 \cdot 10^4 & 0 \\ 0 & 0 & 4.46 \cdot 10^4 \end{bmatrix}$$

$$c1 := \text{eigenvec}\left[B, \lambda_1\right] \qquad c2 := \text{eigenvec}\left[B, \lambda_0\right] \qquad c3 := \text{eigenvec}\left[B, \lambda_2\right]$$

$$c1 = \begin{bmatrix} 0.561614 \\ 0.507972 \\ 0.653111 \end{bmatrix} \qquad c2 = \begin{bmatrix} -0.780495 \\ 0.063256 \\ 0.621953 \end{bmatrix} \qquad c3 = \begin{bmatrix} -0.274621 \\ 0.859048 \\ -0.431995 \end{bmatrix}$$

Define the C matrix which contains the eigenvectors:

$$C := \begin{bmatrix} c1_0 & c2_0 & c3_0 \\ c1_1 & c2_1 & c3_1 \\ c1_2 & c2_2 & c3_2 \end{bmatrix}$$

$$E := N^{-1} \cdot C \qquad E = \begin{bmatrix} 0.005481 & -0.007617 & -0.00268 \\ 0.005481 & 6.825038 \cdot 10^{-4} & 0.009269 \\ 0.005481 & 0.005219 & -0.003625 \end{bmatrix}$$

The resonant frequencies of the system are:

$$w2 := \sqrt{\lambda_0} \qquad w2 = 104.4 \qquad\qquad w3 := \sqrt{\lambda_2} \qquad w3 = 211.2$$

$$f2 := \frac{w2}{[2 \cdot \pi]} \qquad f2 = 16.613248 \qquad\qquad f3 := \frac{w3}{[2 \cdot \pi]} \qquad f3 = 33.605615$$

The Mode shapes can now be found from appropriate normalization of the E matrix.

$$R := \begin{bmatrix} 1 & 1 & 1 \\ \frac{E_{(2,0)}}{E_{(0,0)}} & \frac{E_{(2,1)}}{E_{(0,1)}} & \frac{E_{(2,2)}}{E_{(0,2)}} \\ \frac{E_{(1,0)}}{E_{(0,0)}} & \frac{E_{(1,1)}}{E_{(0,1)}} & \frac{E_{(1,2)}}{E_{(0,2)}} \end{bmatrix}$$

$$R = \begin{bmatrix} 1 & 1 & 1 \\ 1 & -0.685232 & 1.352679 \\ 1 & -0.089604 & -3.458445 \end{bmatrix}$$